ETH
Eidgenössische Technische Hochschule Zürich
Swiss Federal Institute of Technology Zurich

Seminar for Applied Mathematics SAM

Optimal Operator preconditioning for weakly singular operator over 3D screens

R. Hiptmair and C. Jerez-Hanckes and C. Urzúa-Torres

Research Report No. 2017-13
February 2017

Seminar für Angewandte Mathematik
Eidgenössische Technische Hochschule
CH-8092 Zürich
Switzerland

Funding: ETH grant ETH-04 13-2

OPTIMAL OPERATOR PRECONDITIONING FOR WEAKLY SINGULAR OPERATOR OVER 3D SCREENS

RALF HIPTMAIR*, CARLOS JEREZ-HANCKES†, AND CAROLINA URZÚA-TORRES‡

Abstract. In this supplement to [14], we propose a new Calderón-type preconditioner for the weakly singular integral operator for $-\Delta$ on screens in $\mathbb{R}^3$. We introduce a modified hypersingular operator, which is the exact inverse of the weakly singular operator on the unit disk. It forms the foundation for dual-mesh-based operator preconditioning. Applied to low-order boundary element Galerkin discretizations, it achieves h-independent bounded condition numbers. Heuristic extensions to general screens even with non-smooth boundaries are discussed. Their good performance is confirmed by numerical tests.

1. Introduction. This report is the second part of our work on operator preconditioning for Boundary Integral Operators (BIOs) for $-\Delta$ on three-dimensional open surfaces. We therefore consider the following Dirichlet and Neumann boundary value problems on the exterior of an orientable Lipschitz manifold $\Gamma \subset \mathbb{R}^3$, of co-dimension equal to one and boundary $\partial\Gamma$ of positive measure: find U such that

$$\begin{cases} -\Delta U = 0 & \text{in } \Omega := \mathbb{R}^3 \setminus \overline{\Gamma}\,, \\ U = g \quad \text{or} \quad \dfrac{\partial U}{\partial n} = \mu & \text{on } \Gamma\,, \\ U(\mathbf{x}) = \mathcal{O}(\|\mathbf{x}^{-1}\|) & \text{as } \|\mathbf{x}\| \to \infty, \end{cases}$$

where here $\|\cdot\|$ denotes the standard Euclidean norm. This is the simplest case to consider for potential distributions on bounded objects which are infinitely thin in $\mathbb{R}^3$. Such objects are known in the literature as screens. In our first report [14], we focused on the related hard screen problem (Neumann), while here we deal with its soft counterpart (Dirichlet).

A common numerical approach to model and numerically solve problems in unbounded homogeneous domains is the Boundary Element Method (BEM). Its key ingredients are: availability of a fundamental solution and Green's third identity which yields the so-called *integral representation*. In the homogeneous case, the latter allows to reconstruct U over the entire domain using exclusively boundary data via *single and double layer potentials*. When imposing boundary conditions, one derives Boundary Integral Equations (BIEs). In the case of screens, one derives a weakly singular BIE for the Dirichlet BVP, whereas for the Neumann BVP one arrives to a hypersingular BIE. The analysis of the arising Boundary Integral Operators (BIOs) in the framework of Sobolev spaces for screens is available for several problems [31, 30, 27, 3].

In both cases, one faces first-kind BIEs, which lead to ill-conditioned linear systems when discretized by low-order Galerkin BEM on fine meshes. Their solution via iterative solvers becomes prohibitively slow and thus demands preconditioning. For references and further ellaboration on this matter, see the introduction in [14].

The key contribution of this supplementary article is the final resolution of a problem still declared open in [14]: the construction of an exact inverse of the weakly

*Seminar for Applied Mathematics, ETH Zurich, Raemistrasse 101, 8092 Zurich, Switzerland. ralf.hiptmair@sam.math.ethz.ch.

†School of Engineering, Pontificia Universidad Católica de Chile, Av. Vicuña Mackenna 4860, Macul, Santiago, Chile. cjerez@ing.puc.cl. This work was partially funded by Chile CORFO Engineering 2030 program through grant OPEN-UC 201603 and Conicyt Anillo ACT1417.

‡Seminar for Applied Mathematics, ETH Zurich, Raemistrasse 101, 8092 Zurich, Switzerland. carolina.urzua@sam.math.ethz.ch. .

singular integral operator on the unit disk both in terms of a finite part integral operator with a special kernel and in terms of a variational (weak) form in suitable trace spaces. The former is derived in Section 2.2, the latter established in Section 2.2.1. It turns out that this variational form is related to the modified weakly singular operator from [14] in exactly the same way as the weak form of the hypersingular operator can be expressed through that for the weakly singular operator.

Instrumental in the derivation of this variational form of the inverse of the wealy singular operator have been recent yet unpublished results by J.-C.Nédélec [23, 24] also elaborated in the PhD thesis of P.Ramaciotti [26]. They use so-called projected spherical harmonics in order to state series expansions for the kernels of the boundary integral operators and their inverses on the disk. We make use of such relations and prove them in a different way as will be shown in Appendix A.

This report is structured as follows. Section 2.1 yields an inverse of the weakly singular BIO amenable to Galerkin discretization by standard polynomial boundary elements. This can be used for operator preconditioning of the linear systems of equations arising from boundary element discretization of the weakly singular BIE. We investigate this method and various extensions in Section 3 and give ample numerical evidence confirming its efficacy in Section 4. Conclusions are drawn in Section 5 and appendices are provided for detailed proofs.

2. Preliminaries. Let $d = 1, 2, 3$. For a bounded domain $K \subseteq \mathbb{R}^d$, $C^m(K)$, $m \in \mathbb{N}$, denotes the space of m-times differentiable scalar functions on K, and, similarly, for the space of infinitely differentiable, scalar continuous functions we write $C^\infty(K)$. Let $L^p(K)$ denote the class of p-integrable functions over K. Dual spaces are defined in standard fashion with duality products denoted by angular brackets $\langle \cdot\,,\,\cdot \rangle_K$.

Let $\mathcal{O} \in \mathbb{R}^d$, $d = 2, 3$ be open and $s \in \mathbb{R}$. We denote standard Sobolev spaces by $H^s(\mathcal{O})$. For positive s and $\mathcal{O}$ Lipschitz, let $\widetilde{H}^s(\mathcal{O})$ be the space of functions whose extension by zero over a closed domain $\tilde{\mathcal{O}}$ belongs to $H^s(\tilde{\mathcal{O}})$, as in [17]. In particular, the following duality relations hold

$$\widetilde{H}^{-1/2}(\mathcal{O}) \equiv \Big(H^{1/2}(\mathcal{O})\Big)' \qquad \text{and} \qquad H^{-1/2}(\mathcal{O}) \equiv \Big(\widetilde{H}^{1/2}(\mathcal{O})\Big)'. \tag{2.1}$$

2.1. Variational Boundary Integral Equations on the Disk. Throughout this section we focus on the circular disk $\mathbb{D}_a$ with radius $a > 0$, defined as $\mathbb{D}_a := \{\mathbf{x} \in \mathbb{R}^3 : x_3 = 0 \text{ and } \|\mathbf{x}\| < a\}$. Thus, the volume problem domain becomes $\Omega_a := \mathbb{R}^3 \setminus \overline{\mathbb{D}}_a$. Often, we will omit the third coordinate and use the following polar coordinate short notation: $\mathbf{x} = (r_x \cos\theta_x, r_x \sin\theta_x) \in \mathbb{D}_a$.

2.1.1. Weakly Singular Integral Equation. We consider the following singular integral equation: for $g \in H^{1/2}(\mathbb{D}_a)$, we seek a function σ defined on $\mathbb{D}_a$ such that

$$(\mathsf{V}\,\sigma)(\mathbf{y}) := \frac{1}{4\pi} \int_{\mathbb{D}_a} \frac{\sigma(\mathbf{x})}{\|\mathbf{x}-\mathbf{y}\|} d\mathbb{D}_a(\mathbf{x}) = g(\mathbf{y}), \qquad \mathbf{y} \in \mathbb{D}_a, \tag{2.2}$$

The measure $d\mathbb{D}_a(\mathbf{x})$ denotes the surface element in terms of $\mathbf{x} \in \mathbb{D}_a$, equal to $a r_x dr_x d\theta_x$, and the unknown $\sigma \in \widetilde{H}^{-1/2}(\mathbb{D}_a)$ is the jump of the Neumann trace of the solution U of the exterior Dirichlet problem (2.1) when $\Omega = \Omega_a$.

The symmetric variational formulation for (2.2) is: seek $\sigma \in \widetilde{H}^{-1/2}(\mathbb{D}_a)$ such that for $g \in H^{1/2}(\bar{\mathbb{D}}_a)$, it holds

$$\langle \mathsf{V}\,\sigma\,,\,\psi\rangle_{\mathbb{D}_a} := \frac{1}{4\pi} \int_{\mathbb{D}_a} \int_{\mathbb{D}_a} \frac{\sigma(\mathbf{x})\psi(\mathbf{y})}{\|\mathbf{x}-\mathbf{y}\|} d\mathbb{D}_a(\mathbf{x}) d\mathbb{D}_a(\mathbf{y}) = \langle g\,,\,\psi\rangle_{\mathbb{D}_a}, \tag{2.3}$$

for all $\psi \in \widetilde{H}^{-1/2}(\mathbb{D}_a)$.

REMARK 1. *Existence and uniqueness of solution of this problem was proved by Stephan in [30, Thm. 2.7]. Moreover, the bilinear form in* (2.3) *is* $\widetilde{H}^{-1/2}(\Gamma)$*-continuous and elliptic (*cf. *[27, Thm. 3.5.9]). One can show that in this case and for sufficiently smooth screens* Γ*, when approaching the edges* $\partial\Gamma$*, the solutions decay according to the square-root of the distance [4].*

2.2. Modified Hypersingular Singular Integral Operator. We define the *modified* hypersingular operator $\overline{\mathsf{W}}$ as

$$(\overline{\mathsf{W}}g)(\mathbf{x}) := -\frac{2}{\pi^2}\dashint_{\mathbb{D}_a} g(\mathbf{y})K_{\overline{\mathsf{W}}}(\mathbf{x},\mathbf{y})d\mathbb{D}_a(\mathbf{y}), \quad \mathbf{x} \in \mathbb{D}_a, \tag{2.4}$$

with

$$K_{\overline{\mathsf{W}}}(\mathbf{x},\mathbf{y}) := \frac{a}{\|\mathbf{x}-\mathbf{y}\|^2\sqrt{a^2-r_x^2}\sqrt{a^2-r_y^2}} + \frac{S_a(\mathbf{x},\mathbf{y})}{\|\mathbf{x}-\mathbf{y}\|^3}, \quad \mathbf{x} \neq \mathbf{y}, \tag{2.5}$$

and

$$S_a(\mathbf{x},\mathbf{y}) := \tan^{-1}\left(\frac{\sqrt{a^2-r_x^2}\sqrt{a^2-r_y^2}}{a\,\|\mathbf{x}-\mathbf{y}\|}\right), \quad \mathbf{x} \neq \mathbf{y}, \tag{2.6}$$

and where the dashed integral indicates that the expression above is to be interpreted as a Hadamard finite-part integral, with distributional meaning as in [21].

Since $\lim_{\mathbf{x}\to\mathbf{y}} S_a(\mathbf{x},\mathbf{y}) = 4$ when $\mathbf{x}, \mathbf{y} \in \mathbb{D}_a$, the kernel of the standard hypersingular operator W (defined as in [14, Eq. (2.2)]) and the second term in (2.5) have the same hypersingular behavior in the interior of $\mathbb{D}_a$. Also note that $S_a(\mathbf{x},\mathbf{y}) = 0$ if $|\mathbf{x}| = a$ or $|\mathbf{y}| = a$. As a consequence, S_a, though bounded, will be discontinuous on $\partial\mathbb{D}_a \times \partial\mathbb{D}_a$. On the other hand, the first term in (2.5) features a strongly singular kernel in the interior of $\mathbb{D}_a$ and a hypersingular behaviour when $\mathbf{x} = \mathbf{y} \in \partial\mathbb{D}_a$. From these observations we point out that $\overline{\mathsf{W}}$ has a truly hypersingular kernel.

PROPOSITION 2.1. $\overline{\mathsf{W}} : H^{1/2}(\mathbb{D}_a) \to \widetilde{H}^{-1/2}(\mathbb{D}_a)$ *provides an exact inverse of* V.

Key tools for the proof of Proposition 2.1 are some auxiliary results by Li and Rong [19]. First, define the function $\mathsf{p}(\rho,\theta)$ as

$$\mathsf{p}(\rho,\theta) := \frac{1}{2\pi}\sum_{n=-\infty}^{\infty}\rho^{|n|}\mathrm{e}^{in\theta} = \frac{1}{2\pi}\frac{1-\rho^2}{1+\rho^2-2\rho\cos\theta}, \quad \forall\ |\rho| < 1, \tag{2.7}$$

with $\theta \in [0, 2\pi]$ (*cf.* [6, Chap. 1.1]).

THEOREM 2.2 (Thm.1 [19]). *Let* $g \in C^1(\bar{\mathbb{D}}_a)$*. Then, the solution* $\sigma(\mathbf{x})$ *of* (2.2) *can be expressed in terms of a two-dimensional hypersingular integral as follows*

$$\sigma(\mathbf{x}) = -\frac{1}{\pi}\int_{\mathbb{D}_a}\frac{g(\mathbf{y})}{R^3_{\mathbb{D}}(\mathbf{x},\mathbf{y})}d\mathbb{D}_a(\mathbf{y}), \quad \mathbf{x} \in \mathbb{D}_a, \tag{2.8}$$

where

$$\frac{1}{R^3_{\mathbb{D}}(\mathbf{x},\mathbf{y})} := -4\dashint_{\max(r_x,r_y)}^{a}\frac{s^2}{(s^2-r_x^2)^{3/2}(s^2-r_y^2)^{3/2}}\,\mathsf{p}\left(\frac{r_x r_y}{s^2}, \theta_x - \theta_y\right)ds. \tag{2.9}$$

LEMMA 2.1. *Let $a > 0$ and $\mathbf{x}, \mathbf{y} \in \mathbb{D}_a$. If $a \geq s \geq \max(r_x, r_y)$, we find the following primitive*

$$\int \frac{s^2 \, \mathsf{p}\left(\frac{r_x r_y}{s^2}, \theta_x - \theta_y\right)}{(s^2 - r_x^2)^{3/2}(s^2 - r_y^2)^{3/2}} ds = -\frac{1}{2\pi} \left(\frac{s}{\|\mathbf{x}-\mathbf{y}\|^2 \sqrt{s^2 - r_x^2}\sqrt{s^2 - r_y^2}} + \frac{\tan^{-1}\left(\frac{\sqrt{s^2 - r_x^2}\sqrt{s^2 - r_y^2}}{s\|\mathbf{x}-\mathbf{y}\|}\right)}{\|\mathbf{x}-\mathbf{y}\|^3} \right). \tag{2.10}$$

Proof. This can be shown by direct calculation using the following change of variable [6]:

$$\eta := \frac{\sqrt{s^2 - r_x^2}\sqrt{s^2 - r_y^2}}{s}, \qquad \frac{d\eta}{ds} = \frac{s^4 - r_x^2 r_y^2}{\eta s^3},$$

which leads to

$$\int \frac{s^2}{(s^2 - r_x^2)^{3/2}(s^2 - r_y^2)^{3/2}} \frac{1 - r_x^2 r_y^2}{1 + r_x^2 r_y^2 - 2 r_x r_y \cos(\theta_x - \theta_y)} ds = \int \frac{\eta^{-2}}{\|\mathbf{x}-\mathbf{y}\|^2 + \eta^2} d\eta,$$

where

$$\int \frac{\eta^{-2}}{\|\mathbf{x}-\mathbf{y}\|^2 + \eta^2} d\eta = -\frac{1}{\eta \|\mathbf{x}-\mathbf{y}\|^2} - \frac{\tan^{-1}\left(\frac{\eta}{\|\mathbf{x}-\mathbf{y}\|}\right)}{\|\mathbf{x}-\mathbf{y}\|^3}. \tag{2.11}$$

By definition of η the result follows. □

Combining the above elements we can prove the next result.

PROPOSITION 2.3. *The solution of the weakly singular integral equation (2.2) can be written as $\sigma(\mathbf{x}) = (\overline{\mathsf{W}} g)(\mathbf{x})$, for all $\mathbf{x} \in \mathbb{D}_a$, if g is continuously differentiable.*

Proof. Applying Theorem 2.2, we get that the solution to (2.2) can be written as (2.8). Moreover, when $a < \infty$, we may use Lemma 2.1 and write

$$\begin{aligned} -\frac{1}{\pi}\frac{1}{R^3_{\mathbb{D}}(\mathbf{x},\mathbf{y})} &= \frac{4}{\pi} \int_{\max(r_x, r_y)}^{a} \frac{s^2}{(s^2 - r_x^2)^{3/2}(s^2 - r_y^2)^{3/2}} \, \mathsf{p}\left(\frac{r_x r_y}{s^2}, \theta_x - \theta_y\right) ds \\ &= -\frac{2}{\pi^2} fp \left(\frac{s}{\|\mathbf{x}-\mathbf{y}\|^2 \sqrt{s^2 - r_x^2}\sqrt{s^2 - r_y^2}} + \frac{\tan^{-1}\left(\frac{\sqrt{s^2 - r_x^2}\sqrt{s^2 - r_y^2}}{s\|\mathbf{x}-\mathbf{y}\|}\right)}{\|\mathbf{x}-\mathbf{y}\|^3} \right) \Bigg|_{\max(r_x, r_y)}^{a}, \end{aligned}$$

where the finite part (*fp*) of the last expression needs to be considered. This means that we drop the term corresponding to evaluating our primitive (2.10) on the lower bound $\max(r_x, r_y)$, as it becomes infinite.

Hence we get

$$\begin{aligned} -\frac{1}{\pi}\frac{1}{R^3_{\mathbb{D}}(\mathbf{x},\mathbf{y})} &= -\frac{2}{\pi^2} \left(\frac{a}{\|\mathbf{x}-\mathbf{y}\|^2 \sqrt{a^2 - r_x^2}\sqrt{a^2 - r_y^2}} + \frac{S_a(\mathbf{x},\mathbf{y})}{\|\mathbf{x}-\mathbf{y}\|^3} \right) \\ &= -\frac{2}{\pi^2} K_{\overline{\mathsf{W}}}(\mathbf{x},\mathbf{y}), \end{aligned}$$

as stated. □

Finally, we need to extend the above result to $H^{1/2}(\mathbb{D}_a)$. We do this via the following Corollary and subsequent Proposition.

COROLLARY 2.4. $\mathsf{V}\overline{\mathsf{W}} = \mathsf{Id}$ *in* $H^{1/2}(\mathbb{D}_a)$.

Proof. Follows from the previous Proposition combined with density of $C^\infty(\bar{\mathbb{D}}_a)$ in $H^{1/2}(\mathbb{D}_a)$. □

PROPOSITION 2.5. $\overline{\mathsf{W}} : H^{1/2}(\mathbb{D}_a) \to \widetilde{H}^{-1/2}(\mathbb{D}_a)$ *is continuous.*

Proof. Let us assume that $\overline{\mathsf{W}} : H^{1/2}(\mathbb{D}_a) \to \widetilde{H}^{-1/2}(\mathbb{D}_a)$ is not a bounded operator. Then, by virtue of density, there exists a sequence $(g_n)_n \in C^\infty(\bar{\mathbb{D}}_a)$ such that

$$\|g_n\|_{H^{1/2}(\mathbb{D}_a)} = 1, \qquad \left\|\overline{\mathsf{W}} g_n\right\|_{\widetilde{H}^{-1/2}(\mathbb{D}_a)} \to \infty, \text{ as } n \to \infty.$$

Since $\mathsf{V} : \widetilde{H}^{-1/2}(\mathbb{D}_a) \to H^{1/2}(\mathbb{D}_a)$ is an isomorphism, it holds

$$\left\|\overline{\mathsf{W}} g_n\right\|_{\widetilde{H}^{-1/2}(\mathbb{D}_a)} \leq C \left\|\mathsf{V}\overline{\mathsf{W}} g_n\right\|_{H^{1/2}(\mathbb{D}_a)} \underset{(Corollary\ 2.4)}{=} C \|g_n\|_{H^{1/2}(\mathbb{D}_a)},$$

from where we get a contradiction. □

Now we are finally in the position to use the above results and density arguments to conclude the assertion of Proposition 2.1.

COROLLARY 2.6. *The bilinear form* $\left\langle \overline{\mathsf{W}} u\,,\, g \right\rangle_{\mathbb{D}_a}$, $u, g \in H^{1/2}(\mathbb{D}_a)$ *is* $H^{1/2}(\mathbb{D}_a)$*-elliptic and continuous.*

Proof. Follows from continuity and ellipticity of V (*cf.* [27, Thm. 3.5.9]) combined with Proposition 2.1. □

2.2.1. Bilinear Form for the Modified Hypersingular Integral Operator. We note that formula (2.5) is not practical when implementing a Galerkin BEM discretization. We dedicate this section to find a new expression for the bilinear form of $\overline{\mathsf{W}}$ such that its implementation becomes easier.

Let us begin by considering the modified weakly singular operator $\overline{\mathsf{V}}$ given by

$$(\overline{\mathsf{V}}v)(\mathbf{x}) := -\frac{2}{\pi^2} \int_{\mathbb{D}_a} \frac{S_a(\mathbf{x},\mathbf{y})}{\|\mathbf{x}-\mathbf{y}\|} v(\mathbf{y})\, d\mathbb{D}_a(\mathbf{y}), \quad \mathbf{x} \in \mathbb{D}_a,\ v \in H^{-1/2}(\mathbb{D}_a). \tag{2.12}$$

As shown in [14, Section 2.1.2], this BIO renders the exact inverse of the standard hypersingular operator $\mathsf{W} : \widetilde{H}^{1/2}(\mathbb{D}_a) \to H^{-1/2}(\mathbb{D}_a)$.

Let v be a continuously differentiable function over a surface Γ, and let $\tilde{v}$ be an appropriate extension of v into a three-dimensional neighborhood of Γ. Let us introduce the *vectorial* surfacic curl operator [29, p.133] as

$$\underline{\mathrm{curl}}_\Gamma\, v(\mathbf{x}) := \mathbf{n}(\mathbf{x}) \times \nabla \tilde{v}(\mathbf{x}), \tag{2.13}$$

with $\mathbf{n}(\mathbf{x})$ being the outer normal of Γ on $\mathbf{x} \in \Gamma$, and ∇ denoting the standard gradient.

Let us also consider a vector-valued differentiable function $\mathbf{v}(\mathbf{x})$, for $\mathbf{x} \in \Gamma$, and let $\tilde{\mathbf{v}}$ be an appropriate extension of $\mathbf{v}$ into a three-dimensional neighborhood of Γ. Then we also introduce the *scalar* surfacic curl operator [29, p.133] as

$$\mathrm{curl}_\Gamma \mathbf{v}(\mathbf{x}) := \mathbf{n}(\mathbf{x}) \cdot (\nabla \times \tilde{\mathbf{v}}(\mathbf{x})). \tag{2.14}$$

Additionally we denote $\omega(\mathbf{x}) := \sqrt{1-r_x^2}$, $\mathbf{x} \in \mathbb{D}_1$.

PROPOSITION 2.7. *The bilinear form associated to the modified hypersingular operator* $\overline{\mathsf{W}} = \mathsf{V}^{-1}$ *over* $\mathbb{D}_1$ *can be written as*

$$\left\langle \overline{\mathsf{W}} u \, , \, v \right\rangle_{\mathbb{D}_1} = \frac{2}{\pi^2} \int_{\mathbb{D}_1} \int_{\mathbb{D}_1} \frac{S_1(\mathbf{x},\mathbf{y})}{\|\mathbf{x}-\mathbf{y}\|} \, \underline{\mathrm{curl}}_{\mathbb{D}_1,\mathbf{x}} \, u(\mathbf{x}) \cdot \underline{\mathrm{curl}}_{\mathbb{D}_1,\mathbf{y}} \, v(\mathbf{y}) d\mathbb{D}_1(\mathbf{x}) d\mathbb{D}_1(\mathbf{y}), \quad (2.15)$$

for all $u, v \in H^{1/2}_*(\mathbb{D}_1) := \{ v \in H^{1/2}(\mathbb{D}_1) \, : \, \left\langle v \, , \, \omega^{-1} \right\rangle_{\mathbb{D}_1} = 0 \}$.

This result was first reported by Nedélec and Ramaciotti in their spectral study of the BIOs over $\mathbb{D}_1$ and their variational inverses [26]. For the sake of completeness, we introduce the key tools they derived and provide an alternative simpler proof of this proposition in the Appendix A. A proof by means of formal integration by parts remains elusive, as it encounters difficulties due to the finite part integrals involved in the definition of $\overline{\mathsf{W}}$ and its kernel introduced in (2.9).

We also emphasize that the space $H^{1/2}_*(\mathbb{D}_1)$ corresponds to $H^{1/2}(\mathbb{D}_1)/\mathbb{R}$ (see end of Appendix A for further details).

Proposition 2.7 gives us a variational form for $\overline{\mathsf{W}}$ that can be easily implemented. Nevertheless, since we are interested in preconditioning V mapping from $\widetilde{H}^{-1/2}(\mathbb{D}_1)$ to $H^{1/2}(\mathbb{D}_1)$, it is important to observe that the right-hand side of (2.15) maps constants to zero and thus has a non-trivial kernel if considered in the whole $H^{1/2}(\mathbb{D}_1)$ space.

For this reason, (2.15) will not lead to a suitable preconditioner for V. Furthermore, its extension to $H^{1/2}(\mathbb{D}_1)$ does not actually match the bilinear form of $\overline{\mathsf{W}}$ there, which is $H^{1/2}(\mathbb{D}_1)$-elliptic. In order to remedy this situation, we add an appropriate regularizing term coming from the definition of $H^{1/2}_*(\mathbb{D}_1)$ and the following Proposition.

PROPOSITION 2.8. *The following identity holds:*

$$(\overline{\mathsf{W}}1)(\mathbf{y}) = \frac{4}{\pi} \omega^{-1}(\mathbf{y}), \qquad \mathbf{y} \in \mathbb{D}_1. \quad (2.16)$$

The proof can be found in Appendix B. As expected, this result is consistent with the known solutions of (2.2) when the right hand side is $g = 1$ [20].

From this, we see that for u_c constant, $(\overline{\mathsf{W}} u_c)(\mathbf{y})$ is equivalent to

$$(\overline{\mathsf{W}} u_c)(\mathbf{y}) = \frac{2}{\pi^2} \int_{\mathbb{D}_1} u_c(\mathbf{x}) \omega^{-1}(\mathbf{x}) \omega^{-1}(\mathbf{y}) d\mathbb{D}_1(\mathbf{x}), \qquad \mathbf{y} \in \mathbb{D}_1, \quad (2.17)$$

since $\left\langle 1 \, , \, \omega^{-1} \right\rangle_{\mathbb{D}_1} = 2\pi$.

Therefore, by defining the bilinear form:

$$\begin{aligned} \mathsf{b}_{\overline{\mathsf{W}}}(u,v) :=& \frac{2}{\pi^2} \int_{\mathbb{D}_1} \int_{\mathbb{D}_1} \frac{S_1(\mathbf{x},\mathbf{y})}{\|\mathbf{x}-\mathbf{y}\|} \, \underline{\mathrm{curl}}_{\mathbb{D}_1,\mathbf{x}} \, u(\mathbf{x}) \cdot \underline{\mathrm{curl}}_{\mathbb{D}_1,\mathbf{y}} \, v(\mathbf{y}) d\mathbb{D}_1(\mathbf{x}) d\mathbb{D}_1(\mathbf{y}) \\ &+ \frac{2}{\pi^2} \int_{\mathbb{D}_1} \int_{\mathbb{D}_1} \frac{u(\mathbf{x}) v(\mathbf{y})}{\omega(\mathbf{x}) \omega(\mathbf{y})} d\mathbb{D}_1(\mathbf{x}) d\mathbb{D}_1(\mathbf{y}), \quad \forall u, v \in H^{1/2}(\mathbb{D}_1), \end{aligned} \quad (2.18)$$

we have added the required regularization such that (2.16) is preserved. This guarantees that our bilinear form $\mathsf{b}_{\overline{\mathsf{W}}}$ defined in (2.18) is by construction equivalent to the bilinear form arising from our modified hypersingular operator $\overline{\mathsf{W}}$ (2.4) on $H^{1/2}(\mathbb{D}_1)$.

REMARK 2. *Please observe that the chosen regularization to extend the bilinear form* (2.15) *from* $H^{1/2}_*(\Gamma)$ *to* $H^{1/2}(\Gamma)$ *is analogous to the one needed for the modified*

hypersingular operator in 2D [13, eq. (2.11)].

REMARK 3. *For the standard weakly singular and hypersingular operators, the following relation between their kernels holds:*

$$\underbrace{\frac{1}{\|\mathbf{x}-\mathbf{y}\|^3}}_{=:K_{\mathsf{W}}} = \Delta \underbrace{\frac{1}{\|\mathbf{x}-\mathbf{y}\|}}_{=:K_{\mathsf{V}}},$$

while their modified version does not satisfy this relation. Actually, one has [7, eq. (23)]

$$\begin{aligned}\Delta K_{\overline{\mathsf{V}}} &:= -\frac{(2\pi a)\,\mathsf{p}\left(\frac{r_x r_y}{a}, \theta_x-\theta_y\right)}{(a^2-r_y^2)^{3/2}\sqrt{a^2-r_x^2}} + \frac{a}{\|\mathbf{x}-\mathbf{y}\|^2\sqrt{a^2-r_x^2}\sqrt{a^2-r_y^2}} + \frac{S_a(\mathbf{x},\mathbf{y})}{\|\mathbf{x}-\mathbf{y}\|^3} \\ &= -\frac{(2\pi a)\,\mathsf{p}\left(\frac{r_x r_y}{a}, \theta_x-\theta_y\right)}{(a^2-r_y^2)^{3/2}\sqrt{a^2-r_x^2}} + K_{\overline{\mathsf{W}}} \neq K_{\overline{\mathsf{W}}},\end{aligned}$$

where the first term is singular on $\partial\mathbb{D}_a$ and is surprisingly not symmetric. Further investigation should consider the interpretation of this term.

3. Preconditioning Strategy.

3.1. Abstract Operator Preconditioning. Let us consider the continuous bilinear form $\mathsf{a} \in \mathcal{L}(\widetilde{H}^{-1/2}(\Gamma) \times \widetilde{H}^{-1/2}(\Gamma), \mathbb{R})$ induced by V. Following the policy of operator preconditioning [11], we can build our preconditing strategy by finding a continuous bilinear form $\mathsf{b} \in \mathcal{L}(H^{1/2}(\Gamma) \times H^{1/2}(\Gamma), \mathbb{R})$, and finite dimensional spaces $X_h \subset \widetilde{H}^{-1/2}(\Gamma)$ and $Y_h \subset H^{1/2}(\Gamma)$ such that:

- **(P1)** a, b and the L^2-duality pairing t satisfy discrete inf-sup conditions with constants $c_A, c_B, c_T > 0$ respectively, on the corresponding discrete spaces; and,
- **(P2)** $\dim X_h = M = \dim Y_h$.

Choosing any bases of X_h and Y_h, then the associated Galerkin matrices $\mathbf{A}_h, \mathbf{B}_h$, and $\mathbf{T}_h$ satisfy [11, Thm. 2.1]:

$$\kappa(\mathbf{T}_h^{-1}\mathbf{B}_h\mathbf{T}_h^{-T}\mathbf{A}_h) \leq \frac{\|\mathsf{a}\|\|\mathsf{b}\|\|\mathsf{t}\|^2}{c_A c_B c_T^2}\,, \tag{3.1}$$

where κ designates the spectral condition number and the symbol $\|\cdot\|$ must be understood here as operator norms for the induced operators.

REMARK 4. *It was proven that classical "opposite-order" preconditioning leads to a condition number that features a logarithmic growth on 2D screens [22]. We would like to stress the fact that their proof [22, Theorem 4.1] comes from the mismatch of norms between the standard fractional spaces $H^{\pm 1/2}(\Gamma)$ and the tilde ones $\widetilde{H}^{\pm 1/2}(\Gamma)$, with Γ being the screen. Therefore, it is also valid on 3D screens and applies, not only to preconditioning W by V, but to precondition V with W too.*

In order to see this, recall the mapping properties of these BIOs on a screen Γ:

$$\mathsf{V} : \widetilde{H}^{-1/2}(\Gamma) \to H^{1/2}(\Gamma), \qquad \mathsf{W} : \widetilde{H}^{1/2}(\Gamma) \to H^{-1/2}(\Gamma), \tag{3.2}$$

and that the following inverse inequalities hold on shape-regular sequences of BE spaces

$$\|u\|_{\widetilde{H}^{1/2}(\Gamma)} \leq c_1(1+|\log h|)\,\|u\|_{H^{1/2}(\Gamma)}\,, \tag{3.3}$$

$$\|\varphi\|_{\widetilde{H}^{-1/2}(\Gamma)} \leq c_2(1+|\log h|)\,\|\varphi\|_{H^{-1/2}(\Gamma)}\,, \tag{3.4}$$

Fig. 3.1: Barycentric refinement for triangles and quadrilaterals. On the left we illustrate the 6 obtained children elements for a triangular element, while on the right we show the 4 children elements in the case of quadrilaterals. Original primal nodes are in red dots, center of mass is depicted in green diamond and blue x's are used for mid-edge nodes.

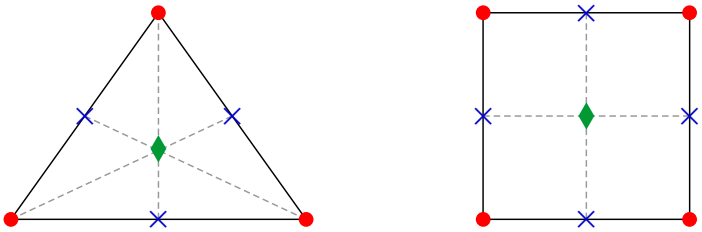

Fig. 3.2: Primal and dual meshes. Black lines show primal elements, dashed gray lines barycentric ones, and blue lines are used to highlight dual cells. Orange dots mark the dofs in X_h and Y_h.

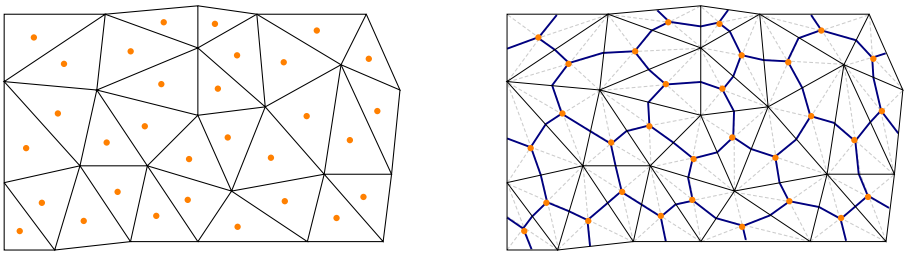

(a) Primal mesh **(b)** Dual mesh

for $u \in \widetilde{H}^{1/2}(\Gamma), \varphi \in \widetilde{H}^{-1/2}(\Gamma)$*, mesh-width* $h \leq 1$ *and with constants* $c_1, c_2 > 0$ *independent of* h *(*cf. *[10, Lemma 2.8] or [12]).*

In the scope of our operator preconditioning theory, these two ingredients together with (3.1) *justify our claim.*

REMARK 5. *If* b *happens to be the exact inverse of* a*, the obtained condition number* (3.1) *will be minimal. However, this is not really required in order to have an optimal preconditioner, and there are several suitable candidates for the bilinear forms* b*.*

3.2. Bounday Element Spaces on Primal and Dual Meshes. We can choose boundary element spaces X_h and Y_h such that they fulfill the condition $M = \dim X_h = \dim Y_h$ by using a dual mesh based on the work of Buffa-Christiansen [2]. Along these lines, we first mesh our screen Γ and denote the resulting primal mesh by Γ_h. Next, we build a barycentric refinement $\overline{\Gamma}_h$ as shown in Figure 3.1. At last, we construct the dual mesh $\widehat{\Gamma}_h$ by combining the barycentric elements, as displayed in Figure 3.2. We refer to [2, 16] for further details.

We construct our discrete spaces by using low-order Lagrangian boundary element

functions, i.e.

$$\begin{aligned} X_h &:= \text{ space of piecewise constant functions on } \Gamma_h, \\ \bar{X}_h &:= \text{ space of piecewise constant functions on } \overline{\Gamma}_h, \\ Y_h &:= \text{ space of continuous piecewise linear functions on } \widehat{\Gamma}_h. \\ \bar{Y}_h &:= \text{ space of continuous piecewise linear functions on } \overline{\Gamma}_h. \end{aligned}$$

Thus $M = \dim X_h = \dim Y_h$ equals the number of cells in Γ_h, as illustrated in Figure 3.2.

Rather than setting our Galerkin matrices directly over $\widehat{\Gamma}_h$, we compute them in the barycentric refinement $\overline{\Gamma}_h$ and define the matrix representation of the inclusion operator $\mathbf{C}_d : \bar{Y}_h \to Y_h$ to build the basis functions of Y_h as linear combinations of barycentric basis functions of $\bar{Y}_h$.

Then, we construct the Galerkin matrix $\overline{\mathbf{W}}_h$ of the modified hypersingular operator $\overline{\mathsf{W}}$ over the dual mesh $\widehat{\Gamma}_h$ as follows: Let $\overline{\mathbf{W}}_b : \bar{Y}_h \to \bar{Y}_h$ be the Galerkin matrix of $\overline{\mathsf{W}}$ computed over the barycentric refinement $\overline{\Gamma}_h$, then we write $\overline{\mathbf{W}}_h = \mathbf{C}_d^T \overline{\mathbf{W}}_b \mathbf{C}_d$.

Analogously, we introduce the matrix representation of the canonical embedding $\mathbf{C}_p : \bar{X}_h \to X_h$ to connect barycentric basis functions corresponding to $\bar{X}_h$ to those of the *primal* basis functions X_h. The construction and representation of these linking matrices are discussed in [16, Sect. 3.3–3.4, case A]. Let us illustrate their use: consider $\mathbf{M}_b : \bar{X}_h \to \bar{Y}_h$ to be the mass matrix computed over the barycentric mesh. By using the above matrices, it is clear that the Galerkin matrix $\mathbf{T}_h$ associated to the L^2-duality pairing t is given by $\mathbf{T}_h = \mathbf{C}_p^T \mathbf{M}_b^T \mathbf{C}_d^T$.

3.3. Stability of Discrete Duality Pairing on Non-Uniform Triangular Meshes. As mentioned in Remark 1, solutions of screen problems have a singular behavior near the boundary, which can be resolved by refining the mesh towards it. This motivates our interest in applying the operator preconditioning strategy to non-uniform meshes. We accomplish this by extending the work developed by O. Steinbach in [28]. Let us begin by introducing some of the notation therein.

As aforementioned, the key instrument is the preservation of the inf-sup condition associated to the dual pairing t, in this case the L^2-inner product over Γ. This requires maintaining the H^1-stability of a generalized L^2-projection $\tilde{Q}_h$, defined via a Petrov-Galerkin approach [28, 16].

With this in mind, let us consider two scenarios:
Case I : $X_h \subset X = \widetilde{H}^{-1/2}(\Gamma)$ and $Y_h \subset Y = H^{1/2}(\Gamma)$,
Case II : $X_h \subset X = H^{1/2}(\Gamma)$ and $Y_h \subset Y = \widetilde{H}^{-1/2}(\Gamma)$.
It is more convenient to first prove the desired inf-sup condition in *Case II*. Once stability is proven there, we can ressort to duality to obtain the inf-sup in the pair of spaces of *Case I*.

ASSUMPTION 3.1. *We consider a shape regular and locally quasi-uniform family of primal meshes* $\{\Gamma_h\}_{h\in\mathbb{H}}$, $h > 0$ *of* Γ, *whose members are labelled by* h *from an index set* $\mathbb{H}$.

Let us consider a given primal mesh Γ_h, and denote the mesh-width of an arbitrary element $\tau_l \in \Gamma_h$ by h_l. We consider *Case II*, and equip $X_h \subset H^{1/2}(\Gamma)$ with the standard locally supported nodal basis functions denoted by $\varphi_k \in X_h$. Due to local quasi-uniformity, for each basis function an associated mesh size $\hat{h}_k$ is introduced,

satisfying

$$\frac{1}{c_Q} \leq \frac{\hat{h}_k}{h_l} \leq c_Q \quad \text{for all } l \text{ such that } \tau_l \cap \text{ supp}\{\varphi_k\} \neq \emptyset,\, k = 1, \ldots, M, \tag{3.5}$$

with a global constant $c_Q \geq 1$. Now, for an arbitrary $\tau_l \in \Gamma_h$, define the set

$$J(l) := \{k \in \{1, ..., M\} \,:\, \text{supp } \{\varphi_k\} \cap \tau_l \neq \emptyset\}. \tag{3.6}$$

Assumption 3.2. *We assume our primal mesh Γ_h satisfies the following local mesh condition:*

$$\frac{51}{7} - \sqrt{\sum_{k_1 \in J(l)} \hat{h}_{k_1} \sum_{k_2 \in J(l)} \hat{h}_{k_2}^{-1}} \geq c_0 > 0 \quad \forall\, \tau_l \in \Gamma_h, \tag{3.7}$$

with a global positive constant c_0 [28, eq. (2.30)].

Theorem 3.3. *Let Assumptions 3.1 and 3.2 be satisfied. Then, for* case I *and* case II *the discrete inf-sup condition:*

$$\sup_{v_h \in Y_h} \frac{|\langle w_h \,,\, v_h \rangle_\Gamma|}{\|v_h\|_Y} \geq \frac{1}{c_s} \|w_h\|_X \,, \qquad \forall\, w_h \in X_h,\, h \in \mathbb{H},\, h > 0. \tag{3.8}$$

holds with a positive constant c_s independent of h.

Proof. Under Assumptions 3.1 and 3.2, Theorems 2.1 and 2.2 in [28] give the inf-sup condition for *case II*. Next, we appeal to an analogue of [28, Lemma 1.7] to define $\widetilde{Q}_h^2 : L^2(\Gamma) \to Y_h$ for a given $u \in L^2(\Gamma)$ as solution of the variational problem

$$\left\langle \widetilde{Q}_h^2 u \,,\, \psi_h \right\rangle_\Gamma = \langle u \,,\, \psi_h \rangle_\Gamma \,, \quad \forall\, \psi_h \in X_h. \tag{3.9}$$

Moreover, following the steps from [28, Thm. 2.1], one can prove that

$$\left\| \widetilde{Q}_h^2 u \right\|_{H^{1/2}(\Gamma)} \leq c \, \|u\|_{H^{1/2}(\Gamma)} \,, \quad \forall u \in H^{1/2}(\Gamma),\, h \in \mathbb{H}. \tag{3.10}$$

Finally, combining these results, we have for all $v_h \in X_h$ that

$$\begin{aligned} \|v_h\|_{\widetilde{H}^{-1/2}(\Gamma)} &= \sup_{0 \neq w \in H^{1/2}(\Gamma)} \frac{|\langle v_h \,,\, w \rangle_\Gamma|}{\|w\|_{H^{1/2}(\Gamma)}} = \sup_{0 \neq w \in H^{1/2}(\Gamma)} \frac{\left| \left\langle v_h \,,\, \widetilde{Q}_h^2 w \right\rangle_\Gamma \right|}{\|w\|_{H^{1/2}(\Gamma)}} \\ &\leq c \sup_{0 \neq w \in H^{1/2}(\Gamma)} \frac{\left| \left\langle v_h \,,\, \widetilde{Q}_h^2 w \right\rangle_\Gamma \right|}{\left\| \widetilde{Q}_h^2 w \right\|_{H^{1/2}(\Gamma)}} \leq c \sup_{0 \neq w_h \in Y_h(\Gamma)} \frac{|\langle v_h \,,\, w_h \rangle_\Gamma|}{\|w_h\|_{H^{1/2}(\Gamma)}}. \end{aligned}$$

as studied. □

We have now all the ingredients to apply the operator preconditioning strategy stated in Section 3.1 over $\mathbb{D}_1$ such that:

Corollary 3.4. *Let Assumptions 3.1 and 3.2 hold. Let $\mathbf{V}_h$ be the Galerkin matrix corresponding to the bilinear form (2.2) over Γ_h. Let $\overline{\mathbf{W}}_h$ be the Galerkin matrix arising from our regularized bilinear form $\mathsf{b}_{\overline{\mathsf{W}}}$ over the dual mesh $\widehat{\Gamma}_h$, and $\mathbf{T}_h$ the matrix representing the L^2-dual pairing constructed as above. Then, when preconditioning $\mathbf{V}_h$ by the matrix product $\overline{\mathbf{P}}_h = \mathbf{T}_h^{-1}\overline{\mathbf{W}}_h\mathbf{T}_h^{-T}$, we obtain*

$$\kappa\left(\overline{\mathbf{P}}_h \mathbf{V}_h\right) \leq C, \tag{3.11}$$

with C a constant independent of h.

3.4. Unit Disk Based Preconditioner for Mapped Screens. We now generalize this preconditioning strategy to more general screens $\Gamma \subset \mathbb{R}^3$ such that there are at least bi-Lipschitz mappings $\boldsymbol{\phi} : \overline{\mathbb{D}}_1 \to \overline{\Gamma}$, so the following norm equivalences hold [21, Thm 3.23]

$$\|\boldsymbol{\phi}^* v\|_{H^1(\mathbb{D}_1)} \approx \|v\|_{H^1(\Gamma)}, \quad \forall v \in H^1(\Gamma), \tag{3.12a}$$

$$\|\boldsymbol{\phi}^* v\|_{L^2(\mathbb{D}_1)} \approx \|v\|_{L^2(\Gamma)}, \quad \forall v \in L^2(\Gamma), \tag{3.12b}$$

where $\boldsymbol{\phi}^* v$ is the pullback of the function v.

REMARK 6. *As a consequence of the bi-Lipschitz mapping $\boldsymbol{\phi} : \overline{\mathbb{D}}_1 \to \overline{\Gamma}$, Γ will be an orientable $C^{0,1}$- manifold with boundary $\partial\Gamma$. Moreover, $\boldsymbol{\phi}$ allows us to use the fact that the spaces $\widetilde{H}^{1/2}(\Gamma)$, $H^{1/2}(\Gamma)$, $H^{-1/2}(\Gamma)$, and $\widetilde{H}^{-1/2}(\Gamma)$ are invariant under the pullback $\boldsymbol{\phi}^* : L^2(\Gamma) \to L^2(\mathbb{D}_1)$.*

For the sake of clarity, we introduce additional notation for this section. Let us write $\mathsf{V}_{\mathbb{D}_1}$ to denote the weakly singular operator on the unit disk, and V_Γ for that on $\Gamma = \boldsymbol{\phi}(\mathbb{D}_1)$, i.e.

$$(\mathsf{V}_\Gamma \sigma)(\mathbf{x}) := \frac{1}{4\pi} \int_\Gamma \frac{\sigma(\mathbf{y})}{\|\mathbf{x} - \mathbf{y}\|} d\Gamma(\mathbf{y}), \quad \mathbf{x} \in \Gamma,\ \sigma \in \widetilde{H}^{-1/2}(\Gamma). \tag{3.13}$$

It can be pulled back to $\mathbb{D}_1$ using the parametrization:

$$(\mathsf{V}_\Gamma^* \boldsymbol{\phi}^* \sigma)(\boldsymbol{\phi}(\hat{\mathbf{x}})) := \frac{1}{4\pi} \int_{\mathbb{D}_1} \frac{(\boldsymbol{\phi}^* \sigma)(\hat{\mathbf{y}}) \sqrt{\det\,(D\boldsymbol{\phi}(\hat{\mathbf{y}})^T D\boldsymbol{\phi}(\hat{\mathbf{y}}))}}{\|\boldsymbol{\phi}(\hat{\mathbf{x}}) - \boldsymbol{\phi}(\hat{\mathbf{y}})\|} d\mathbb{D}_1(\hat{\mathbf{y}}), \quad \hat{\mathbf{x}} \in \mathbb{D}_1, \tag{3.14}$$

where $D\boldsymbol{\phi}(\hat{\mathbf{x}})$ denotes the Jacobian of $\boldsymbol{\phi}$ on $\hat{\mathbf{x}}$, and $\boldsymbol{\phi}^*(\sigma) \in \widetilde{H}^{-1/2}(\mathbb{D}_1)$.

In the operator preconditioning context, let us define the bilinear forms:

$$\mathsf{a}(\hat{\sigma}, \hat{\varphi}) = \langle \mathsf{V}_\Gamma^* \hat{\sigma}, \hat{\varphi} \rangle_{\mathbb{D}_1}, \quad \hat{\sigma}, \hat{\varphi} \in \widetilde{H}^{-1/2}(\mathbb{D}_1), \tag{3.15}$$

$$\mathsf{b}(\hat{u}, \hat{v}) = \langle \overline{\mathsf{W}}_{\mathbb{D}_1} \hat{u}, \hat{v} \rangle_{\mathbb{D}_1}, \quad \hat{u}, \hat{v} \in H^{1/2}(\mathbb{D}_1), \tag{3.16}$$

where $\overline{\mathsf{W}}_{\mathbb{D}_1}$ denotes the modified hypersingular operator over $\mathbb{D}_1$. From Proposition 2.6, we know that b is $H^{1/2}(\mathbb{D}_1)$-elliptic and continuous.

Now, we can use (3.12) and interpolation arguments to get

$$\|\boldsymbol{\phi}^* v\|_{H^{1/2}(\mathbb{D}_1)} \approx \|v\|_{H^{1/2}(\Gamma)}, \quad \forall v \in H^{1/2}(\Gamma), \tag{3.17}$$

and the definition of dual norm to derive

$$\|\hat{\sigma}\|_{\widetilde{H}^{-1/2}(\mathbb{D}_1)} \approx \left\|\boldsymbol{\phi}^{-*} \hat{\sigma}\right\|_{\widetilde{H}^{-1/2}(\Gamma)}, \quad \forall \hat{\sigma} \in \widetilde{H}^{-1/2}(\mathbb{D}_1), \tag{3.18}$$

where superscript -* denotes the inverse of the pullback. From the latter norm equivalence and the properties of V_Γ, one can deduce the $\widetilde{H}^{-1/2}(\mathbb{D}_1)$-ellipticity and continuity of a.

$$\mathsf{a}(\hat{\sigma}, \hat{\sigma}) = \left\langle \mathsf{V}_\Gamma \boldsymbol{\phi}^{-*} \hat{\sigma}, \boldsymbol{\phi}^{-*} \hat{\sigma} \right\rangle_\Gamma \geq c \left\|\boldsymbol{\phi}^{-*} \hat{\sigma}\right\|^2_{\widetilde{H}^{-1/2}(\Gamma)} \approx c \|\hat{\sigma}\|^2_{\widetilde{H}^{-1/2}(\mathbb{D}_1)},$$

for all $\hat{\sigma} \in \widetilde{H}^{-1/2}(\mathbb{D}_1)$.

These properties of a and b, combined with the $\widetilde{H}^{-1/2}(\mathbb{D}_1) - H^{1/2}(\mathbb{D}_1)$-stability of the L^2-pairing, give the following corollary.

COROLLARY 3.5. *$\overline{\mathsf{W}}_{\mathbb{D}_1}$ still induces a suitable bilinear form to build an h-asymptotically optimal preconditioner for V_Γ^* adopting the procedures of our preconditioning strategy.*

REMARK 7. *Note that*

$$\overline{\mathsf{W}}_{\mathbb{D}_1}\,\mathsf{V}_\Gamma^* = \mathsf{Id} + \overline{\mathsf{W}}_{\mathbb{D}_1}(\mathsf{V}_\Gamma^* - \mathsf{V}_{\mathbb{D}_1}) \;:\; \widetilde{H}^{-1/2}(\mathbb{D}_1) \to \widetilde{H}^{-1/2}(\mathbb{D}_1), \tag{3.19}$$

is also continuous.

Corollary 3.5 guarantees that the condition number bound (3.1) will be constant, albeit affected by a constant depending on $\boldsymbol{\phi}$ and the distortion effected by it. Later on, this will be reflected in our numerical experiments by means of a pre-asymptotic phase in which the behavior of the preconditioner is not as good as expected. Motivated by this numerical drawback, the following two subsections discuss some heuristic modifications to improve the preconditioner performance.

3.5. Shape-aware Preconditioners.

3.5.1. Case of Flat Screens. We consider general surfaces that allow polar angle para-metrization of their boundary, i.e. boundaries that can be described by a function $a(\theta), \theta \in [0, 2\pi]$. In this case, we can use

$$S_\Gamma(\mathbf{x},\mathbf{y}) = \tan^{-1}\left(\frac{\sqrt{a(\theta_x)^2 - r_x^2}\sqrt{a(\theta_y)^2 - r_y^2}}{\sqrt{a(\theta_x)a(\theta_y)}\,\|\mathbf{x}-\mathbf{y}\|}\right), \quad \text{for } \mathbf{x} \neq \mathbf{y},\ \mathbf{x},\mathbf{y} \in \Gamma, \tag{3.20}$$

to construct an approximation of V^{-1} (see [14, Sect. 3.6] for further motivation). We point out that the flat screen needs not be the result of a transformed unit disk via a bi-Lipschitz mapping as in the previous subsection. However, a piecewise Lipschitz transformation is still required.

The approximation of the bilinear form related to $\overline{\mathsf{W}}$ that we pursue is

$$\begin{aligned}\mathsf{b}^{\Gamma}_{\overline{\mathsf{W}}}(u,v) :=& \frac{2}{\pi^2}\int_\Gamma\int_\Gamma \frac{S_\Gamma(\mathbf{x},\mathbf{y})}{\|\mathbf{x}-\mathbf{y}\|^3}\,\underline{\mathrm{curl}}_{\Gamma,\mathbf{x}}\,u(\mathbf{x})\cdot\underline{\mathrm{curl}}_{\Gamma,\mathbf{y}}\,v(\mathbf{y})d\Gamma(\mathbf{x})d\Gamma(\mathbf{y}) \\ &+ \alpha_{\overline{\mathsf{W}}}\langle u\,,\,1\rangle_\Gamma\langle v\,,\,1\rangle_\Gamma\,,\end{aligned} \tag{3.21}$$

for $u, v \in H^{1/2}(\Gamma)$, and with $\alpha_{\overline{\mathsf{W}}} \in \mathbb{R}_+$ bounded.

Here, we have additionally replaced the function ω^{-1} by the constant 1 in the correction term for implementation simplicity. We justify this choice on account of the fact that we will use PCG to solve the arising system and said method will not perceive a significant difference among these two regularizations. Moreover, this choice will reduce computations considerably when compared to the original choice in (2.18).

3.5.2. Case of Parametrized Screens. Let us consider an open surface Γ defined by a C^1-diffeomorphism $\boldsymbol{\phi} : \bar{\mathbb{D}}_1 \to \overline{\Gamma}$. In this situation we can approximate $S_1(\mathbf{x},\mathbf{y})$ by

$$S_{\boldsymbol{\phi}}(\mathbf{x},\mathbf{y}) := \tan^{-1}\left(\frac{\sqrt{1-\left\|\boldsymbol{\phi}^{-1}(\mathbf{x})\right\|^2}\sqrt{1-\left\|\boldsymbol{\phi}^{-1}(\mathbf{y})\right\|^2}}{\sqrt{g_{\boldsymbol{\phi}^{-1}}(\mathbf{x})g_{\boldsymbol{\phi}^{-1}}(\mathbf{y})}\,\|\mathbf{x}-\mathbf{y}\|}\right), \tag{3.22}$$

for $\mathbf{x} \neq \mathbf{y}$, and where $g_{\boldsymbol{\phi}^{-1}}(\mathbf{x})$ is the Gram determinant of $\boldsymbol{\phi}^{-1}$ on $\mathbf{x}$ [14, Sect. 3.7].

This expression is somehow analogous to the approach developed in Section 3.5.1 with $a(\theta_x) = \boldsymbol{\phi}(\frac{\mathbf{x}}{\|\mathbf{x}\|})$. Again, we will base our preconditioner on an approximate bilinear form for the modified hypersingular operator $\overline{\mathsf{W}}$. However, this time we replace $S_\Gamma(\mathbf{x}, \mathbf{y})$ in (3.21) by $S_{\boldsymbol{\phi}}(\mathbf{x}, \mathbf{y})$.

4. Numerical Experiments. We compare the performace of our preconditioner $\overline{\mathbf{P}}_h := \mathbf{T}_h^{-1}\overline{\mathbf{W}}_h\mathbf{T}_h^{-T}$ with diagonal preconditioning –denoted by $\mathbf{D}_h^{-1}$–, and opposite-order operator preconditioning arising from using the standard hypersingular operator W, i.e. $\mathbf{P}_h := \mathbf{T}_h^{-1}\mathbf{W}_h\mathbf{T}_h^{-T}$. It is worth mentioning that the bilinear form arising from W also needs a regularization term [13, Sect. 5.1], chosen in the same way as for $\overline{\mathbf{P}}_h$. This means we add a term equal

$$\alpha_{\mathsf{W}} \left\langle u\,,\, \omega^{-1} \right\rangle_{\mathbb{D}_1} \left\langle v\,,\, \omega^{-1} \right\rangle_{\mathbb{D}_1}, \qquad u, v \in H^{1/2}(\mathbb{D}_1), \tag{4.1}$$

in the case of the unit disk $\mathbb{D}_1$, or

$$\alpha_{\mathsf{W}} \left\langle u\,,\, 1 \right\rangle_{\Gamma} \left\langle v\,,\, 1 \right\rangle_{\Gamma}, \qquad u, v \in H^{1/2}(\Gamma), \tag{4.2}$$

for general Γ, where $\alpha_{\mathsf{W}} \in \mathbb{R}_+$ bounded.

Currently, we do not have a rule of thumb to choose the parameters α_{W} and $\alpha_{\overline{\mathsf{W}}}$. In fact, we selected each one of them empirically in the following way: First, we set an initial guess for both parameters and computed the resulting full Galerkin matrices and their spectra. By changing parameter values, we then seeked to locate eigenvalues related to the regularizing term inside the remaining spectra, thus preventing an artificial enlargement of condition numbers. Consequently, they do not alter the performance of the preconditioners and allow us to make fair comparisons between $\overline{\mathbf{P}}_h$ and $\mathbf{P}_h$. As our eigenvalues cluster around one, we have found that for the disk, $\alpha_{\mathsf{W}} = \alpha_{\overline{\mathsf{W}}} = \frac{1}{2\pi}$ is a good choice, while for general screens Γ, a good initial guess is given by the inverse of the area of the screen.

Numerical experiments were implemented employing BETL2 [15] and the required meshes generated with `Gmsh` [8] using polygonal approximation of the boundaries. The measured condition numbers were computed via the ratio of the maximum and minimum eigenvalues. All required BEM operators were constructed with 12 quadrature points[1].

For fine meshes, local low-rank compression of the BE matrices had to be used. Specifically, BETL2 uses AHMED for its ACA implementation. The parameters used for these experiments correspond to BETL default ones, i.e., tolerance of 10^{-5} and admissibility $\eta = 0.9$.

In most numerical experiments we provide two tables. The one on the left, entitled *No approximation*, contains the spectral condition numbers computed using standard BETL routines to construct the matrices and MATLAB to obtain the condition numbers. The table on the right *ACA with Lanczos* gives the spectral condition numbers κ and the number of PCG iterations *It* for matrices constructed with the ACA routines. Moreover, *with Lanczos* indicates that for this case the condition numbers were calculated using Preconditioned Conjugate Gradient (PCG) with the Lanczos algorithm [9, Ch.9–10]. We use PCG with a tolerance of 10^{-5} for the relative residual norm, initial guess equal to zero and, as right hand side, we considered a

[1]Except for the rank-one regularizations (4.2) and (2.18), where BETL2's default number of quadrature points was used, i.e., 7 for the mass-matrix and 25 for $\langle 1\,,\, \omega^{-1} \rangle$.

vector that had entries $+1$ in its upper half, -1 for the remaining components. Since a sufficiently precise computation of the eigenvalues usually requires a larger Krylov subspace and hence more PCG iterations, the algorithm continues iterating until the difference between the newly computed condition number and the old one is less or equal to 10^{-4} for two times consecutively.

4.1. Unit Disk. Tables 4.1.1 and 4.1.2 show the preconditioning results over a disk with two different triangular meshes and parameters $\alpha_{\mathsf{W}} = \alpha_{\overline{\mathsf{W}}} = \frac{1}{2\pi}$. In both tables, the condition numbers displayed with ACA differ in some cases from those obtained using dense BE matrices without any approximation. Table 4.1.3 reveals that here the approximation error comes mainly from ACA, although Lanczos lacks accuracy in some cases. In spite of this, we observe in Tables 4.1.1 and 4.1.2 that the condition numbers achieved by $\overline{\mathbf{P}}_h$ hardly increase with respect to the number of elements and are asymptotically smaller than those of $\mathbf{P}_h$. Nevertheless, the gain in terms of number of PCG iterations is not significant.

Table 4.1.1: Results for $\mathbf{V}_h$ over the unit disk with **quasi-uniform triangular** meshes.

(a) No approximation

N	$\kappa(\mathbf{D}_h^{-1}\mathbf{V}_h)$	$\kappa(\mathbf{P}_h\mathbf{V}_h)$	$\kappa(\overline{\mathbf{P}}_h\mathbf{V}_h)$
64	23.91	3.07	2.41
256	50.39	3.19	2.47
1024	102.61	3.52	2.61

(b) ACA with Lanczos

N	$\mathbf{D}_h^{-1}\mathbf{V}_h$		$\mathbf{P}_h\mathbf{V}_h$		$\overline{\mathbf{P}}_h\mathbf{V}_h$	
	κ	It	κ	It	κ	It
64	22.55	13	2.72	7	2.24	6
256	49.41	20	2.84	7	2.48	6
1024	102.28	27	3.22	7	2.63	7
4096	206.81	40	3.85	8	2.72	7
16384	413.67	57	4.69	10	2.87	7

Table 4.1.2: Results for $\mathbf{V}_h$ over the unit disk with **non-uniform triangular** meshes A.

(a) No approximation

N	$\kappa(\mathbf{D}_h^{-1}\mathbf{V}_h)$	$\kappa(\mathbf{P}_h\mathbf{V}_h)$	$\kappa(\overline{\mathbf{P}}_h\mathbf{V}_h)$
96	25.72	5.93	5.58
384	55.55	4.16	3.62
1536	110.82	4.99	3.95

(b) ACA with Lanczos

N	$\mathbf{D}_h^{-1}\mathbf{V}_h$		$\mathbf{P}_h\mathbf{V}_h$		$\overline{\mathbf{P}}_h\mathbf{V}_h$	
	κ	It	κ	It	κ	It
96	25.72	17	5.73	10	5.66	11
384	55.55	22	3.41	8	3.69	9
1536	110.82	32	4.14	9	3.82	9
6144	230.08	44	5.01	10	4.06	10

Table 4.1.3: Results for $\mathbf{V}_h$ over the unit disk for **ACA with Matlab**.

(a) Quasi-uniform meshes

N	$\kappa(\mathbf{D}_h^{-1}\mathbf{V}_h)$	$\kappa(\mathbf{P}_h\mathbf{V}_h)$	$\kappa(\overline{\mathbf{P}}_h\mathbf{V}_h)$
64	23.91	2.73	2.24
256	50.39	2.85	2.48
1024	102.61	3.22	2.63

(b) Non-uniform meshes A

N	$\kappa(\mathbf{D}_h^{-1}\mathbf{V}_h)$	$\kappa(\mathbf{P}_h\mathbf{V}_h)$	$\kappa(\overline{\mathbf{P}}_h\mathbf{V}_h)$
96	25.72	5.99	5.66
384	55.55	3.41	3.69
1536	110.82	4.14	4.08

A third triangular mesh of the unit disk is also studied in Table 4.1.4, again with parameters $\alpha_{\mathsf{W}} = \alpha_{\overline{\mathsf{W}}} = \frac{1}{2\pi}$. This time, each mesh is generated with local refinement on the boundary such that the meshwidth on $\partial\mathbb{D}_1$ is half of the one of the previous mesh. The condition numbers are just as expected. Moreover, this time we can

see that our preconditioner $\overline{\mathbf{P}}_h$ not only achieves an almost constant κ, but also its number of PCG iterations starts having a real advantage over those of $\mathbf{P}_h$.

Table 4.1.4: Results for $\mathbf{V}_h$ over the unit disk with **non-uniform triangular** meshes B.

(a) κ with no approximation

N	$\mathbf{D}_h^{-1}\mathbf{V}_h$	$\mathbf{P}_h\mathbf{V}_h$	$\overline{\mathbf{P}}_h\mathbf{V}_h$
162	33.09	4.29	4.07
506	51.23	4.32	4.04
1052	64.43	4.73	4.00
2150	79.70	5.64	4.04

(b) ACA with Lanczos

N	h_{min}	$\mathbf{D}_h^{-1}\mathbf{V}_h$		$\mathbf{P}_h\mathbf{V}_h$		$\overline{\mathbf{P}}_h\mathbf{V}_h$	
		κ	It	κ	It	κ	It
162	0.05677	33.09	20	4.06	10	4.10	10
506	0.0244	51.23	28	4.11	11	4.04	11
1052	0.0124	64.43	33	4.70	12	4.00	12
2150	0.0059	79.70	42	5.59	14	4.04	12
4260	0.0030	96.09	50	6.83	16	4.37	14
8398	0.0015	113.61	59	7.92	19	4.53	15
16546	0.0008	130.95	68	9.00	21	4.46	15

Fig. 4.1: Locally refined triangular meshes

(a) The coarsest mesh A was created using the functions `Attraction` and `Threshold` iteratively in `Gmsh`. This means the mesh size is a *piecewise linear* function of the distance to the disk's boundary. The subsequent meshes were obtained by standard refinement in `Gmsh`.

(b) Each mesh B was constructed with the functions `Attraction` and `Matheval` in `Gmsh`, where the evaluated function was the *continuous* distance to the boundary of the disk plus a parameter $h_* > 0$. The subsequent meshes were obtained by halving h_* and thus the minimum meshwidth on the boundary.

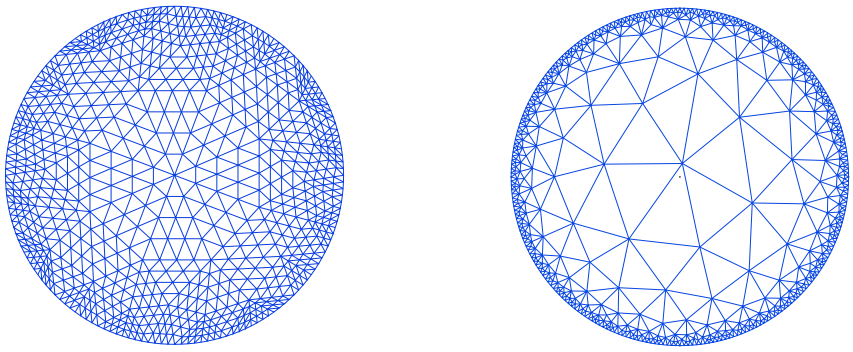

4.2. Unit Disk Based Preconditioner for Mapped Screens. In this section we study the preconditioning results achieved when applying the approach described in Section 3.4. This means that $\mathbf{V}_h$ corresponds to the Galerkin matrix of the weakly singular operator mapped from the disk to the target screen Γ via $\boldsymbol{\phi}$, $\overline{\mathbf{P}}_h$ is constructed on the disk, i.e. using (2.18), whereas $\mathbf{P}_h$ comes from the standard hypersingular operator mapped from $\mathbb{D}_1$ to Γ. We denote by $\alpha_{\overline{\mathsf{W}}}$ the constant chosen for the regularization in $\overline{\mathbf{W}}_h$ and α_{W} for the one of $\mathbf{W}_h$. In these experiments, we considered $\alpha_{\overline{\mathsf{W}}} = \frac{1}{2\pi}$ and $\alpha_{\mathsf{W}} = 0.3$.

Tables 4.2.1, 4.2.2, and 4.2.3 exhibit the preconditioning results for three differ-

ent shapes mapped from the unit disk. In all of them, we see how the opposite-order preconditioner $\mathbf{P}_h$ displays the expected logarithmic growth while our proposal shows a small rise that seems to be less pronounced the larger the mesh. We believe this reflects a pre-asymptotic phase together with numerical errors introduced by quadrature and the ACA approximation. Naturally, this behaviour is also depicted in the number of PCG iterations. Whereas the number of PCG counts for $\mathbf{P}_h$ increases with respect to N, those of $\overline{\mathbf{P}}_h$ remain constant in the last two levels for all considered mappings.

Table 4.2.1: Results for $\mathbf{V}_h$ over mapped screens with **quasi-uniform triangular** meshes. $\overline{\mathbf{P}}_h$ built using unit disk based preconditioner. $\boldsymbol{\phi}(\mathbf{x}) = (x_0, x_1, x_0 + x_1)^T$.

(a) No approximation

N	$\kappa(\mathbf{D}_h^{-1}\mathbf{V}_h)$	$\kappa(\mathbf{P}_h\mathbf{V}_h)$	$\kappa(\overline{\mathbf{P}}_h\mathbf{V}_h)$
64	24.15	3.44	3.24
256	51.69	4.17	3.28
1024	108.95	4.92	3.45

(b) ACA with Lanczos

N	$\mathbf{D}_h^{-1}\mathbf{V}_h$		$\mathbf{P}_h\mathbf{V}_h$		$\overline{\mathbf{P}}_h\mathbf{V}_h$	
	κ	It	κ	It	κ	It
64	24.15	14	3.17	7	3.02	7
256	51.65	22	4.17	8	3.28	8
1024	108.97	30	4.92	9	3.45	8
4096	223.37	43	5.76	10	3.61	9
16384	435.05	59	6.70	12	3.72	9

Table 4.2.2: Results for $\mathbf{V}_h$ over mapped screens with **quasi-uniform triangular** meshes. $\overline{\mathbf{P}}_h$ built using unit disk based preconditioner. $\boldsymbol{\phi}(\mathbf{x}) = (x_0, x_1, x_0^2 + x_1^2)^T$.

(a) No approximation

N	$\kappa(\mathbf{D}_h^{-1}\mathbf{V}_h)$	$\kappa(\mathbf{P}_h\mathbf{V}_h)$	$\kappa(\overline{\mathbf{P}}_h\mathbf{V}_h)$
64	25.97	1.88	4.85
256	54.86	2.20	5.29
1024	111.73	2.56	5.60

(b) ACA with Lanczos

N	$\mathbf{D}_h^{-1}\mathbf{V}_h$		$\mathbf{P}_h\mathbf{V}_h$		$\overline{\mathbf{P}}_h\mathbf{V}_h$	
	κ	It	κ	It	κ	It
64	24.22	13	1.88	5	4.25	9
256	53.55	21	2.20	6	4.83	10
1024	110.98	30	2.56	7	5.21	11
4096	228.14	41	3.05	8	5.47	12
16384	462.54	60	3.69	8	5.66	12

Table 4.2.3: Results for $\mathbf{V}_h$ over mapped screens with **quasi-uniform triangular** meshes. $\overline{\mathbf{P}}_h$ built using unit disk based preconditioner. $\boldsymbol{\phi}(\mathbf{x}) = (x_0, x_1, x_0 x_1)^T$.

(a) No approximation

N	$\kappa(\mathbf{D}_h^{-1}\mathbf{V}_h)$	$\kappa(\mathbf{P}_h\mathbf{V}_h)$	$\kappa(\overline{\mathbf{P}}_h\mathbf{V}_h)$
64	24.29	3.12	2.95
256	51.36	3.69	2.74
1024	104.65	4.38	2.80

(b) ACA with Lanczos

N	$\mathbf{D}_h^{-1}\mathbf{V}_h$		$\mathbf{P}_h\mathbf{V}_h$		$\overline{\mathbf{P}}_h\mathbf{V}_h$	
	κ	It	κ	It	κ	It
64	24.29	14	3.11	11	2.38	7
256	50.33	21	3.68	8	2.55	7
1024	104.49	29	4.36	9	2.78	7
4096	211.30	42	5.16	10	2.96	8
16384	423.25	57	6.16	11	3.08	8

4.3. Shape-aware Preconditioner for Flat Screens. We present numerical results to illustrate the approach proposed in Section 3.5.1. In other words, $\mathbf{V}_h$ corresponds to the matrix coming from the weakly singular operator on the flat screen Γ, $\mathbf{P}_h$ comes from the standard hypersingular operator over Γ, and $\overline{\mathbf{P}}_h$ is constructed using (3.21).

Tables 4.3.1 and 4.3.2 give the numerical results for preconditioning over a square screen over two different triangular meshes and specify the parameters α_{W} and $\alpha_{\overline{\mathsf{W}}}$ considered for $\mathbf{P}_h$ and $\overline{\mathbf{P}}_h$, respectively.

Table 4.3.1: Results for $\mathbf{V}_h$ over a **square** screen with **quasi-uniform triangular** meshes. $\overline{\mathbf{P}}_h$ built using shape-aware preconditioner for flat screens. $\alpha_{\mathsf{W}} = \alpha_{\overline{\mathsf{W}}} = 0.3$

(a) No approximation

N	$\kappa(\mathbf{D}_h^{-1}\mathbf{V}_h)$	$\kappa(\mathbf{P}_h\mathbf{V}_h)$	$\kappa(\overline{\mathbf{P}}_h\mathbf{V}_h)$
64	25.63	3.38	3.35
256	51.99	4.30	3.71
1024	104.29	5.31	3.94

(b) ACA with Lanczos

N	$\mathbf{D}_h^{-1}\mathbf{V}_h$		$\mathbf{P}_h\mathbf{V}_h$		$\overline{\mathbf{P}}_h\mathbf{V}_h$	
	κ	It	κ	It	κ	It
64	25.63	11	3.38	4	3.35	4
256	52.00	18	4.30	6	3.71	6
1024	104.29	25	5.31	7	3.94	6
4096	208.65	37	6.41	9	4.10	6
16384	417.32	51	7.64	8	4.21	6

Once again, we observe some differences between the standard and ACA approaches. However, when outputting the ACA matrices and computing the condition numbers with MATLAB, we get results close to the standard case. We therefore conclude that the error is introduced by the Lanczos algorithm. For the quasi-uniform mesh, there is a slight increase in the condition number that is probably coming from numerical error. In the non-uniform case, the slope decreases but it is not as small. As before, this is also reflected in the number of PCG iterations obtained with $\overline{\mathbf{P}}_h$, which, although asymptotically constant, are not significantly smaller than those achieved by $\mathbf{P}_h$.

Table 4.3.2: Results for $\mathbf{V}_h$ over a **square** screen with **locally refined** meshes. $\overline{\mathbf{P}}_h$ built using shape-aware preconditioner for flat screens. $\alpha_{\mathsf{W}} = \alpha_{\overline{\mathsf{W}}} = 0.3$

(a) No approximation

N	$\kappa(\mathbf{D}_h^{-1}\mathbf{V}_h)$	$\kappa(\mathbf{P}_h\mathbf{V}_h)$	$\kappa(\overline{\mathbf{P}}_h\mathbf{V}_h)$
108	29.66	3.81	4.38
432	59.84	4.73	5.11
1728	120.02	5.78	5.64

(b) ACA with Lanczos

N	$\mathbf{D}_h^{-1}\mathbf{V}_h$		$\mathbf{P}_h\mathbf{V}_h$		$\overline{\mathbf{P}}_h\mathbf{V}_h$	
	κ	It	κ	It	κ	It
108	29.66	16	3.81	8	4.26	9
432	59.84	24	4.73	10	4.98	10
1728	120.02	33	5.78	11	5.52	10
6912	241.51	46	6.94	12	5.59	12
27648	484.43	63	8.19	13	5.92	12

As a second example, we consider three different triangles. Table 4.3.3 provides the condition numbers over an equilateral triangle, Table 4.3.4 shows the results for an isosceles rectangular triangle, and finally the condition numbers obtained for a general triangle with angles $30^\circ - 60^\circ - 90^\circ$ are contained in Table 4.3.5. In these three situations, the standard choice $\alpha_{\overline{\mathsf{W}}} = \alpha_{\mathsf{W}} = 0.3$ leads to unsatisfactory results for both preconditioners. Since the resulting spectra showed that this could be improved by using other values of $\alpha_{\overline{\mathsf{W}}}$ and α_{W}, the Tables (on the right) report the results corresponding to the most convenient values for each operator using no approximation.

Tables 4.3.6–4.3.8 contain the results using ACA with Lanczos and these new values of $\alpha_{\overline{\mathsf{W}}}$ and α_{W}. There we see that $\mathbf{P}_h$ achieves condition numbers with the expected logarithmic growth, while $\overline{\mathbf{P}}_h$ also exhibits a growth that becomes less pronounced for larger N. However, we note that these results are less impressive than for other shapes. Moreover, the PCG counts for $\overline{\mathbf{P}}_h$ are, in most cases, sligthly worse than the number of iterations obtained with $\mathbf{P}_h$. Our preconditioner performs particularly poorly for the general triangle. Futhermore, Figure 4.2 shows that the clustering for the general triangle is not good independently of the chosen $\alpha_{\overline{\mathsf{W}}}$.

Table 4.3.3: Results for $\mathbf{V}_h$ over **equilateral triangle** screen with **quasi-uniform triangular** meshes. $\overline{\mathbf{P}}_h$ built using shape-aware preconditioner for flat screens.

(a) $\alpha_{\mathsf{W}} = \alpha_{\overline{\mathsf{W}}} = 0.3$

N	$\kappa(\mathbf{D}_h^{-1}\mathbf{V}_h)$	$\kappa(\mathbf{P}_h\mathbf{V}_h)$	$\kappa(\overline{\mathbf{P}}_h\mathbf{V}_h)$
74	25.34	28.36	27.55
296	53.11	30.19	30.45
1184	107.96	31.73	32.76

(b) $\alpha_{\mathsf{W}} = 0.05,\ \alpha_{\overline{\mathsf{W}}} = 0.01$

N	$\kappa(\mathbf{D}_h^{-1}\mathbf{V}_h)$	$\kappa(\mathbf{P}_h\mathbf{V}_h)$	$\kappa(\overline{\mathbf{P}}_h\mathbf{V}_h)$
74	25.34	5.35	6.33
296	53.11	6.08	7.27
1184	107.96	7.23	8.06

Table 4.3.4: Results for $\mathbf{V}_h$ over **right isosceles triangle** screen with **quasi-uniform triangular** meshes. $\overline{\mathbf{P}}_h$ built using shape-aware preconditioner for flat screens.

(a) $\alpha_{\mathsf{W}} = \alpha_{\overline{\mathsf{W}}} = 0.3$

N	$\kappa(\mathbf{D}_h^{-1}\mathbf{V}_h)$	$\kappa(\mathbf{P}_h\mathbf{V}_h)$	$\kappa(\overline{\mathbf{P}}_h\mathbf{V}_h)$
60	22.04	6.66	8.89
240	46.50	8.90	10.63
960	94.53	11.36	11.96

(b) $\alpha_{\mathsf{W}} = 0.3,\ \alpha_{\overline{\mathsf{W}}} = 0.1$

N	$\kappa(\mathbf{D}_h^{-1}\mathbf{V}_h)$	$\kappa(\mathbf{P}_h\mathbf{V}_h)$	$\kappa(\overline{\mathbf{P}}_h\mathbf{V}_h)$
60	22.04	6.66	8.72
240	46.50	8.90	10.39
960	94.53	11.36	11.69

Table 4.3.5: Results for $\mathbf{V}_h$ over **general triangle** screen with **quasi-uniform triangular** meshes. $\overline{\mathbf{P}}_h$ built using shape-aware preconditioner for flat screens.

(a) $\alpha_{\mathsf{W}} = \alpha_{\overline{\mathsf{W}}} = 0.3$

N	$\kappa(\mathbf{D}_h^{-1}\mathbf{V}_h)$	$\kappa(\mathbf{P}_h\mathbf{V}_h)$	$\kappa(\overline{\mathbf{P}}_h\mathbf{V}_h)$
32	14.49	14.11	18.39
128	31.82	20.15	22.18
512	70.41	27.10	28.73

(b) $\alpha_{\mathsf{W}} = 0.4,\ \alpha_{\overline{\mathsf{W}}} = 0.3$

N	$\kappa(\mathbf{D}_h^{-1}\mathbf{V}_h)$	$\kappa(\mathbf{P}_h\mathbf{V}_h)$	$\kappa(\overline{\mathbf{P}}_h\mathbf{V}_h)$
32	14.49	15.29	18.39
128	31.82	20.13	22.18
512	70.41	27.08	28.73

Table 4.3.6: ACA with Lanczos results for $\mathbf{V}_h$ over **equilateral triangle** screen with **quasi-uniform triangular** meshes. $\overline{\mathbf{P}}_h$ built using shape-aware preconditioner. $\alpha_{\mathsf{W}} = 0.05,\ \alpha_{\overline{\mathsf{W}}} = 0.01$

N	$\mathbf{D}_h^{-1}\mathbf{V}_h$		$\mathbf{P}_h\mathbf{V}_h$		$\overline{\mathbf{P}}_h\mathbf{V}_h$	
	κ	It	κ	It	κ	It
74	25.34	15	5.35	10	6.29	11
296	52.77	22	6.08	11	7.29	13
1184	107.96	31	7.21	12	8.07	14
4736	217.54	43	8.80	13	8.77	14
18944	437.61	59	10.58	15	9.36	14

Fig. 4.2: Eigenvalue distribution for **general triangle** screen. The spectrum of the matrix $\mathbf{V}_h$ is shown in black, while that of $\mathbf{V}_h$ preconditioned by $\mathbf{W}_h$ is depicted in red. The one corresponding to $\overline{\mathbf{W}}_h$ is in blue. We observe that the bottom part of the spectrum of $\overline{\mathbf{W}}_h\mathbf{V}_h$ remains unclustered independently of the choice of $\alpha_{\overline{W}}$. This allow us to conclude that the deterioration of the performance of $\overline{\mathbf{P}}_h$ does not come from the rank-1 regularization.

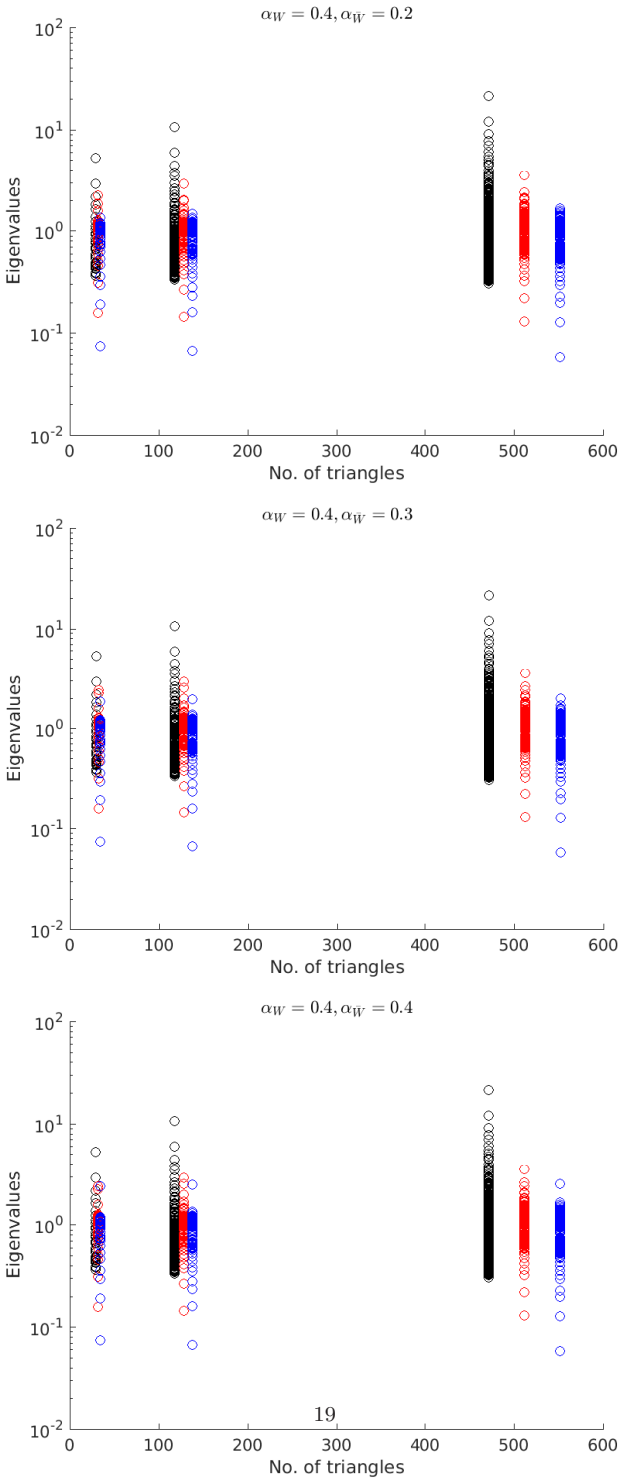

Table 4.3.7: ACA with Lanczos results for $\mathbf{V}_h$ over **isosceles triangle** screen with **quasi-uniform triangular** meshes. $\overline{\mathbf{P}}_h$ built using shape-aware preconditioner. $\alpha_{\mathsf{W}} = 0.3$, $\alpha_{\overline{\mathsf{W}}} = 0.1$

N	$\mathbf{D}_h^{-1}\mathbf{V}_h$		$\mathbf{P}_h\mathbf{V}_h$		$\overline{\mathbf{P}}_h\mathbf{V}_h$	
	κ	It	κ	It	κ	It
60	22.04	14	6.51	10	8.72	14
240	46.50	21	8.90	12	10.39	16
960	94.47	29	11.36	13	11.69	17
3840	190.05	41	13.97	15	12.77	17
15360	381.03	55	16.76	17	13.68	18

Table 4.3.8: ACA with Lanczos results for $\mathbf{V}_h$ over **general triangle** screen with **quasi-uniform triangular** meshes. $\overline{\mathbf{P}}_h$ built using shape-aware preconditioner. $\alpha_{\mathsf{W}} = 0.4$, $\alpha_{\overline{\mathsf{W}}} = 0.3$

N	$\mathbf{D}_h^{-1}\mathbf{V}_h$		$\mathbf{P}_h\mathbf{V}_h$		$\overline{\mathbf{P}}_h\mathbf{V}_h$	
	κ	It	κ	It	κ	It
32	14.49	13	15.29	12	24.88	13
128	31.73	20	20.17	16	28.94	17
512	70.93	28	27.05	19	33.80	21
2048	147.34	38	34.23	21	38.22	23
8192	300.20	53	41.42	24	41.85	26

4.4. Shape-aware Preconditioner for Parametrized Screens. We finally consider the same setting as in the previous subsection but now $\overline{\mathbf{P}}_h$ follows the cue from subsubsection 3.5.2 with parameters $\alpha_{\mathsf{W}} = \alpha_{\overline{\mathsf{W}}} = 0.3$ for the sake of simplicity.

For comparison purposes, Tables 4.4.1, 4.4.2, and 4.4.4 illustrate the results obtained for the same mappings studied in subsection 4.2. From this, we validate our results for the two first columns, and, additionally, remark that the approximation proposed is sometimes succesful in lowering the bound for the condition number, but in other situations is not much better.

Nonetheless, the data in Tables 4.4.1–4.4.6 reveals that our shape-aware preconditioner $\overline{\mathbf{P}}_h$ achieves condition numbers κ that are practically h-independent. Still, this optimality in terms of condition numbers does not meaningfully reduce the number of PCG iterations when compared to the opposite-order preconditioner $\mathbf{P}_h$.

Table 4.4.1: Results for $\mathbf{V}_h$ over parametrized screens with **quasi-uniform triangular** meshes. $\overline{\mathbf{P}}_h$ built using shape-aware preconditioner. $\boldsymbol{\phi}(\mathbf{x}) = (x_0, x_1, x_0 + x_1)^T$.

(a) No approximation

N	$\kappa(\mathbf{D}_h^{-1}\mathbf{V}_h)$	$\kappa(\mathbf{P}_h\mathbf{V}_h)$	$\kappa(\overline{\mathbf{P}}_h\mathbf{V}_h)$
64	24.15	3.44	3.48
256	51.69	4.17	4.02
1024	108.95	4.92	4.26

(b) ACA with Lanczos

N	$\mathbf{D}_h^{-1}\mathbf{V}_h$		$\mathbf{P}_h\mathbf{V}_h$		$\overline{\mathbf{P}}_h\mathbf{V}_h$	
	κ	It	κ	It	κ	It
64	24.15	14	3.17	7	3.48	7
256	51.67	22	4.17	8	4.02	8
1024	108.94	30	4.92	9	4.26	9
4096	223.40	43	5.76	10	4.39	9
16384	435.05	58	6.70	12	4.54	9

Table 4.4.2: Results for $\mathbf{W}_h$ over parametrized screens with **quasi-uniform triangular** meshes. $\overline{\mathbf{P}}_h$ built using shape-aware preconditioner. $\boldsymbol{\phi}(\mathbf{x}) = (x_0, x_1, x_0^2 + x_1^2)^T$.

(a) No approximation

N	$\kappa(\mathbf{D}_h^{-1}\mathbf{V}_h)$	$\kappa(\mathbf{P}_h\mathbf{V}_h)$	$\kappa(\overline{\mathbf{P}}_h\mathbf{V}_h)$
64	26.12	1.89	2.24
256	54.97	2.19	2.72
1024	111.79	2.59	2.93

(b) ACA with Lanczos

N	$\mathbf{D}_h^{-1}\mathbf{V}_h$		$\mathbf{P}_h\mathbf{V}_h$		$\overline{\mathbf{P}}_h\mathbf{V}_h$	
	κ	It	κ	It	κ	It
64	24.33	13	1.89	6	2.24	6
256	53.62	21	2.19	6	2.72	7
1024	111.02	30	2.57	7	2.92	8
4096	228.16	41	3.06	8	3.05	8
16384	462.61	60	3.70	8	3.16	8

Table 4.4.3: Results for $\mathbf{V}_h$ over parametrized screens with **quasi-uniform triangular** meshes. $\overline{\mathbf{P}}_h$ built using shape- aware preconditioner. $\boldsymbol{\phi}(\mathbf{x}) = (x_0, x_1, \frac{x_0^2+x_1^2}{2})^T$.

(a) No approximation

N	$\kappa(\mathbf{D}_h^{-1}\mathbf{V}_h)$	$\kappa(\mathbf{P}_h\mathbf{V}_h)$	$\kappa(\overline{\mathbf{P}}_h\mathbf{V}_h)$
64	24.68	2.93	2.46
256	52.05	3.43	2.74
1024	105.94	4.03	2.87

(b) ACA with Lanczos

N	$\mathbf{D}_h^{-1}\mathbf{V}_h$		$\mathbf{P}_h\mathbf{V}_h$		$\overline{\mathbf{P}}_h\mathbf{V}_h$	
	κ	It	κ	It	κ	It
64	23.20	13	2.92	7	2.46	7
256	50.93	21	3.41	8	2.74	7
1024	105.40	27	4.01	8	2.87	8
4096	213.11	40	4.74	9	2.97	8
16384	427.56	59	5.66	10	3.12	8

Table 4.4.4: Results for $\mathbf{V}_h$ over parametrized screens with **quasi-uniform triangular** meshes. $\overline{\mathbf{P}}_h$ built using shape-aware preconditioner. $\boldsymbol{\phi}(\mathbf{x}) = (x_0, x_1, x_0x_1)^T$.

(a) No approximation

N	$\kappa(\mathbf{D}_h^{-1}\mathbf{V}_h)$	$\kappa(\mathbf{P}_h\mathbf{V}_h)$	$\kappa(\overline{\mathbf{P}}_h\mathbf{V}_h)$
64	24.42	3.22	2.77
256	51.44	3.77	3.01
1024	104.70	4.43	3.19

(b) ACA with Lanczos

N	$\mathbf{D}_h^{-1}\mathbf{V}_h$		$\mathbf{P}_h\mathbf{V}_h$		$\overline{\mathbf{P}}_h\mathbf{V}_h$	
	κ	It	κ	It	κ	It
64	24.42	14	3.20	8	2.77	7
256	51.44	21	3.75	8	3.00	8
1024	104.54	29	4.41	9	3.16	8
4096	211.33	42	5.19	10	3.26	8
16384	423.26	57	6.18	11	3.43	9

Table 4.4.5: Results for $\mathbf{V}_h$ over parametrized screens with **quasi- uniform triangular** meshes. $\overline{\mathbf{P}}_h$ built using shape-aware preconditioner $\boldsymbol{\phi}(\mathbf{x}) = (x_0, x_1, \exp(x_0 + x_1))^T$.

(a) No approximation

N	$\kappa(\mathbf{D}_h^{-1}\mathbf{V}_h)$	$\kappa(\mathbf{P}_h\mathbf{V}_h)$	$\kappa(\overline{\mathbf{P}}_h\mathbf{V}_h)$
64	24.68	5.34	4.99
256	58.86	6.89	6.60
1024	136.45	8.26	7.82

(b) ACA with Lanczos

N	$\mathbf{D}_h^{-1}\mathbf{V}_h$		$\mathbf{P}_h\mathbf{V}_h$		$\overline{\mathbf{P}}_h\mathbf{V}_h$	
	κ	It	κ	It	κ	It
64	24.71	15	5.34	9	4.99	9
256	58.80	23	6.90	10	6.60	11
1024	136.67	34	8.25	12	7.81	12
4096	302.01	48	9.64	13	8.79	13
16384	562.32	66	11.20	15	9.50	13

5. Conclusion. We have developed operator preconditioning on three-dimensional screens using a new hypersingular integral operator that supplies the exact inverse for the weakly singular operator on disks. We have proved that our approach accom-

Table 4.4.6: Results for $\mathbf{V}_h$ over parametrized screens with **quasi-uniform triangular** meshes. $\overline{\mathbf{P}}_h$ built using shape- aware preconditioner. $\boldsymbol{\phi}(\mathbf{x}) = (x_0, x_1, \exp(\frac{x_0+x_1}{2}))^T$.

(a) No approximation

N	$\kappa(\mathbf{D}_h^{-1}\mathbf{V}_h)$	$\kappa(\mathbf{P}_h\mathbf{V}_h)$	$\kappa(\overline{\mathbf{P}}_h\mathbf{V}_h)$
64	24.02	3.47	2.66
256	50.73	4.10	3.02
1024	104.09	4.82	3.20

(b) ACA with Lanczos

N	$\mathbf{D}_h^{-1}\mathbf{V}_h$		$\mathbf{P}_h\mathbf{V}_h$		$\overline{\mathbf{P}}_h\mathbf{V}_h$	
	κ	It	κ	It	κ	It
64	24.02	14	3.47	8	2.66	8
256	50.73	22	4.10	9	3.02	8
1024	104.07	31	4.82	10	3.20	8
4096	212.45	42	5.66	11	3.31	8
16384	420.95	57	6.64	12	3.47	9

plishes h-independent condition numbers for parametrized screens, with remarkable success for non-uniform meshes. Moreover, their performances depend on the extent of deformation of the screen Γ with respect to the unit disk $\mathbb{D}_1$. We indicated that the resulting condition numbers may be rather large depending on the transformation $\boldsymbol{\phi}$. In order to overcome the possibly degraded performance of our approach, we proposed two heuristic alternatives for preconditioning on a general screen. The asymptotic optimality of our preconditioners has been investigated via exhaustive numerical experiments with respect to both uniform and locally refined meshes. We have confirmed that the our proposal achieves the expected performance in all studied shapes except the so-called *general triangle*. Further analysis is necessary to fine-tune the selection among our preconditioner and heuristic approaches.

REFERENCES

[1] H. Bateman and A. Erdélyi, *Higher transcendental functions*, McGraw-Hill, 1952.

[2] A. Buffa and S. Christiansen, *A dual finite element complex on the barycentric refinement*, Mathematics of Computation, 76 (2007), pp. 1743–1769.

[3] A. Buffa and S. H. Christiansen, *The electric field integral equation on Lipschitz screens: definitions and numerical approximation*, Numer. Math., 94 (2003), pp. 229–267.

[4] M. Costabel, M. Dauge, and R. Duduchava, *Asymptotics without logarithmic terms for crack problems*, Comm. Partial Differential Equations, 28 (2003), pp. 869–926.

[5] *NIST Digital Library of Mathematical Functions*. http://dlmf.nist.gov/, Release 1.0.10 of 2015-08-07. Online companion to [25].

[6] V. I. Fabrikant, *Mixed boundary value problems of potential theory and their applications in engineering*, vol. 68 of Mathematics and its Applications, Kluwer Academic Publishers Group, Dordrecht, 1991.

[7] ———, *Exact solution of tangential contact problem for a circular domain*, J. Mech. Phys. Solids, 45 (1997), pp. 113–134.

[8] C. Geuzaine and J.-F. Remacle, *Gmsh: A 3-D finite element mesh generator with built-in pre- and post-processing facilities*, Internat. J. Numer. Methods Engrg., 79 (2009), pp. 1309–1331.

[9] G. H. Golub and C. F. Van Loan, *Matrix computations*, Johns Hopkins Studies in the Mathematical Sciences, Johns Hopkins University Press, Baltimore, MD, third ed., 1996.

[10] N. Heuer, *Preconditioners for the p-version of the boundary element Galerkin method in* $\mathbb{R}^3$, habilitation, Uni Hannover, 1998.

[11] R. Hiptmair, *Operator preconditioning*, Computers and Mathematics with Applications, 52 (2006), pp. 699–706.

[12] R. Hiptmair, C. Jerez-Hanckes, and S. Mao, *Extension by zero in discrete trace spaces: inverse estimates*, Math. Comp., 84 (2015), pp. 2589–2615.

[13] R. Hiptmair, C. Jerez-Hanckes, and C. Urzúa-Torres, *Mesh-independent operator preconditioning for boundary elements on open curves.*, SIAM J. Numerical Analysis, 52 (2014), pp. 2295–2314.

[14] ———, *Optimal operator preconditioning for hypersingular operator over 3d screens*,

Tech. Rep. 2016-09, Seminar for Applied Mathematics, ETH Zürich, Switzerland, 2016. https://www.sam.math.ethz.ch/sam_reports/reports_final/reports2016/2016-09_rev1.pdf.
[15] R. Hiptmair and L. Kielhorn, BETL - *A generic boundary element template library*, tech. rep., SAM - Seminar for Applied Mathematics, ETH Zurich., 2012. https://www.sam.math.ethz.ch/sam_reports/reports_final/reports2012/2012-36.pdf.
[16] R. Hiptmair and C. Urzúa-Torres, *Dual Mesh Operator Preconditioning On 3D Screens: Low-Order Boundary Element Discretization.*, Tech. Rep. 2016-14, Seminar for Applied Mathematics, ETH Zürich, Switzerland, 2016. https://www.sam.math.ethz.ch/sam_reports/reports_final/reports2016/2016-14.pdf.
[17] C. Jerez-Hanckes and J. Nédélec, *Explicit variational forms for the inverses of integral logarithmic operators over an interval*, SIAM Journal on Mathematical Analysis, 44 (2012), pp. 2666–2694.
[18] S. Krenk, *A circular crack under asymmetric loads and some related integral equations*, Journal of Applied Mechanics, 46 (1979), pp. 821–826.
[19] X.-F. Li and E.-Q. Rong, *Solution of a class of two-dimensional integral equations*, J. Comput. Appl. Math., 145 (2002), pp. 335–343.
[20] P. A. Martin, *Exact solution of some integral equations over a circular disc*, J. Integral Equations Appl., 18 (2006), pp. 39–58.
[21] W. McLean, *Strongly Elliptic Systems and Boundary Integral Equations*, Cambridge University Press, Cambridge, UK, 2000.
[22] W. McLean and O. Steinbach, *Boundary element preconditioners for a hypersingular integral equations on an interval*, Adv. Comp. Math., 11 (1999), pp. 271–286.
[23] J.-C. Nédélec, *About some operators on the unit disc related to the laplacian equation*, in Journées Singulières Augmentées, August 2013. Available at https://jsa2013.sciencesconf.org/conference/jsa2013/T52.pdf.
[24] J.-C. Nédélec and P. Ramaciotti, *Inverse boundary integral operator on the disk for the laplace problem*, (2017). In preparation.
[25] F. W. J. Olver, D. W. Lozier, R. F. Boisvert, and C. W. Clark, eds., *NIST Handbook of Mathematical Functions*, Cambridge University Press, New York, NY, 2010. Print companion to [5].
[26] P. Ramaciotti, *Aspects Théoriques et Numériques des Phénomènes de Propagation d'Ondes dans Domaines de Géométrie Complexe et Applications à la Télédétection*, PhD thesis, Université Paris-Saclay/PUC Chile, 2016. To appear.
[27] S. Sauter and C. Schwab, *Boundary Element Methods*, vol. 39 of Springer Series in Computational Mathematics, Springer, Heidelberg, 2010.
[28] O. Steinbach, *Stability estimates for hybrid coupled domain decomposition methods*, vol. 1809 of Lecture Notes in Mathematics, Springer-Verlag, Berlin, 2003.
[29] ———, *Numerical approximation methods for elliptic boundary value problems: Finite and boundary elements*, Springer, New York, 2008. Finite and boundary elements, Translated from the 2003 German original.
[30] E. Stephan, *Boundary integral equations for screen problems in* $\mathbb{R}^3$, Integral Equations and Operator Theory, 10 (1987), pp. 236–257.
[31] E. P. Stephan, *A boundary integral equation method for three-dimensional crack problems in elasticity*, Math. Methods Appl. Sci., 8 (1986), pp. 609–623.
[32] P. Wolfe, *Eigenfunctions of the integral equation for the potential of the charged disk*, Journal of Mathematical Physics, 12 (1971), pp. 1215–1218.

Appendix A. Proof of Proposition 2.7.

We begin by systematically introducing some key definitions and results on the unit disk $\mathbb{D}_1$. When needed, we provide a short proof for the results reported in [26, Chap. 2].

Definition A.1 (**Nedélec's Projected Spherical Harmonics (PSH) over** $\mathbb{D}_1$ [23, eq.(75)]). *For $l, m \in \mathbb{N}_0$ such that $|m| \leq l$, we introduce*

$$y_l^m(\mathbf{x}) := \gamma_l^m e^{im\theta_x} \mathbb{P}_l^m(\sqrt{1-r_x^2}), \qquad \gamma_l^m := (-1)^m \sqrt{\frac{(2l+1)}{4\pi}\frac{(l-m)!}{(l+m)!}}. \tag{A.1}$$

PSH over $\mathbb{D}_1$ satisfy the following orthogonality identity [23, eq.(79)]

$$\int_{\mathbb{D}_1} \frac{y_{l_1}^{m_1}(\mathbf{y})\overline{y_{l_2}^{m_2}}(\mathbf{y})}{\omega(\mathbf{y})} d\mathbb{D}_1(\mathbf{y}) = \frac{1}{2}\delta_{l_1}^{l_2}\delta_{m_1}^{m_2}, \tag{A.2}$$

where $\delta_{(\cdot)}^{(\cdot)}$ is the Kronecker delta and $\omega(\mathbf{y}) = \sqrt{1-r_y^2}$ as in Section 2.2.1.

PROPOSITION A.1. *[32] The weakly singular operator* V *over* $\mathbb{D}_1$ *satisfies the following generalized eigenvalue problem:*

$$(\mathsf{V}\frac{y_l^m}{\omega})(\mathbf{x}) = \frac{1}{4}\lambda_l^m y_l^m(\mathbf{x}), \quad l+m \text{ even}, \tag{A.3}$$

with $\lambda_l^m := \dfrac{\Gamma\left(\frac{l+m+1}{2}\right)\Gamma\left(\frac{l-m+1}{2}\right)}{\Gamma\left(\frac{l+m+2}{2}\right)\Gamma\left(\frac{l-m+2}{2}\right)}$, *and* Γ *being the Gamma function.*

PROPOSITION A.2. *[18] The hypersingular operator* W *over* $\mathbb{D}_1$ *satisfies the following generalized eigenvalue problem:*

$$(\mathsf{W}\, y_l^m)(\mathbf{x}) = \frac{1}{\lambda_l^m}\frac{y_l^m(\mathbf{x})}{\omega(\mathbf{x})}, \quad l+m \text{ odd}, \tag{A.4}$$

with λ_l^m *as in Proposition A.1.*

REMARK 8. *Propositions A.1 and A.2 nicely show how, in the case of a disk, the usual* V *and* W *have opposite symbols but* $\mathsf{W}\,\mathsf{V} \neq \frac{1}{4}\,\mathsf{Id}$ *due to their mapping properties. This is characterized here by the parity of the corresponding generalized eigenfunctions.*

PROPOSITION A.3 ([26, Sect. 2.7][2]). *The kernels of* $\mathsf{V}, \mathsf{W}, \overline{\mathsf{V}}, \overline{\mathsf{W}}$ *have the following* symmetric *series expansions on* $\mathbb{D}_1$

$$K_{\mathsf{V}}(\mathbf{x},\mathbf{y}) := \frac{1}{4\pi}\frac{1}{\|\mathbf{x}-\mathbf{y}\|} = \sum_{l=0}^{\infty}\sum_{\substack{m=-l \\ l+m \text{ even}}}^{l} \frac{\lambda_l^m}{4}\left(y_l^m(\mathbf{x})\overline{y_l^m}(\mathbf{y}) + \overline{y_l^m}(\mathbf{x})y_l^m(\mathbf{y})\right). \tag{A.5}$$

$$K_{\overline{\mathsf{V}}}(\mathbf{x},\mathbf{y}) := \sum_{l=0}^{\infty}\sum_{\substack{m=-l \\ l+m \text{ odd}}}^{l} \lambda_l^m\left(y_l^m(\mathbf{x})\overline{y_l^m}(\mathbf{y}) + \overline{y_l^m}(\mathbf{x})y_l^m(\mathbf{y})\right). \tag{A.6}$$

$$K_{\mathsf{W}}(\mathbf{x},\mathbf{y}) := \frac{1}{4\pi}\frac{1}{\|\mathbf{x}-\mathbf{y}\|^3} = \sum_{l=0}^{\infty}\sum_{\substack{m=-l \\ l+m \text{ odd}}}^{l} \frac{1}{\lambda_l^m}\left(\frac{y_l^m(\mathbf{x})}{\omega(\mathbf{x})}\frac{\overline{y_l^m}(\mathbf{y})}{\omega(\mathbf{y})} + \frac{\overline{y_l^m}(\mathbf{x})}{\omega(\mathbf{x})}\frac{y_l^m(\mathbf{y})}{\omega(\mathbf{y})}\right) \tag{A.7}$$

$$K_{\overline{\mathsf{W}}}(\mathbf{x},\mathbf{y}) := \sum_{l=0}^{\infty}\sum_{\substack{m=-l \\ l+m \text{ even}}}^{l} \frac{4}{\lambda_l^m}\left(\frac{y_l^m(\mathbf{x})}{\omega(\mathbf{x})}\frac{\overline{y_l^m}(\mathbf{y})}{\omega(\mathbf{y})} + \frac{\overline{y_l^m}(\mathbf{x})}{\omega(\mathbf{x})}\frac{y_l^m(\mathbf{y})}{\omega(\mathbf{y})}\right). \tag{A.8}$$

Proof. The proof for the standard BIOs' kernels follows from Proposition A.1 and Proposition A.2 combined with the orthogonality of the projected spherical harmonics (A.2).

[2]Note that in Ramaciotti's notation: $\lambda_l^m = \begin{cases} \dfrac{1}{\alpha_l^m}, & l+m \text{ odd}, \\ \dfrac{4}{\beta_l^m}, & l+m \text{ even} \end{cases}$.

From (A.3), we can additionally find the generalized eigenvalue problem associated to its unique inverse operator $\overline{\mathsf{W}} = \mathsf{V}^{-1}$ over $\mathbb{D}_1$

$$(\overline{\mathsf{W}} y_l^m)(\mathbf{x}) = \frac{4}{\lambda_l^m} \frac{y_l^m(\mathbf{x})}{\omega(\mathbf{x})}, \tag{A.9}$$

and use again the orthogonality property to get (A.8). The result for $K_{\overline{\mathsf{V}}}$ can be obtained analogously from (A.4). □

DEFINITION A.2 (L^2**-weighted spaces** [23, sl. 36–37] [26, Def.2.7.8–2.7.9]). *Let us define the spaces $L^2_{1/\omega}(\mathbb{D}_1)$ and $L^2_{\omega}(\mathbb{D}_1)$ as the L^2-spaces induced by the weighted inner products*

$$(u, v)_{1/\omega} = \int_{\mathbb{D}_1} u(\mathbf{x}) \overline{v(\mathbf{x})} \omega(\mathbf{x})^{-1} d\mathbb{D}_1(\mathbf{x}), \tag{A.10}$$

and

$$(u, v)_{\omega} = \int_{\mathbb{D}_1} u(\mathbf{x}) \overline{v(\mathbf{x})} \omega(\mathbf{x}) d\mathbb{D}_1(\mathbf{x}), \tag{A.11}$$

respectively.

PROPOSITION A.4 ([23, sl. 36–37][26, Prop 2.7.8–2.7.9]). *We have that*

- $\{y_l^m \,:\, l+m \text{ odd}\}$ *and* $\{y_l^m \,:\, l+m \text{ even}\}$ *are both orthogonal bases for* $L^2_{1/\omega}$.
- $\{\omega^{-1} y_l^m \,:\, l+m \text{ odd}\}$ *and* $\{\omega^{-1} y_l^m \,:\, l+m \text{ even}\}$ *are both orthogonal bases for* L^2_{ω}.

PROPOSITION A.5 ([26, Sect. 2.7.4]).

(i) $u \in \widetilde{H}^{1/2}(\mathbb{D}_1)$ *can be expanded on the basis* $\{y_l^m \,:\, l+m \,\mathbf{odd}\}$ *of* $L^2_{1/\omega}$*:*

$$u(\mathbf{x}) = \sum_{l=0}^{\infty} \sum_{m=-l}^{l} u_l^m y_l^m(\mathbf{x}), \quad u_l^m = (u, y_l^m)_{1/\omega}, \quad l+m \text{ odd}. \tag{A.12}$$

(ii) $g \in H^{1/2}(\mathbb{D}_1)$ *can be expanded on the basis* $\{y_l^m \,:\, l+m \,\mathbf{even}\}$ *of* $L^2_{1/\omega}$ *:*

$$g(\mathbf{x}) = \sum_{l=0}^{\infty} \sum_{m=-l}^{l} g_l^m y_l^m(\mathbf{x}), \quad g_l^m = (g, y_l^m)_{1/\omega}, \quad l+m \text{ even}. \tag{A.13}$$

(iii) $v \in H^{-1/2}(\mathbb{D}_1)$ *can be expanded on the basis* $\{y_l^m \omega^{-1} \,:\, l+m \,\mathbf{odd}\}$ *of* L^2_{ω}*:*

$$v(\mathbf{x}) = \sum_{l=0}^{\infty} \sum_{m=-l}^{l} v_l^m \frac{y_l^m(\mathbf{x})}{\omega(\mathbf{x})}, \quad v_l^m = (v, \omega^{-1} y_l^m)_{\omega}, \quad l+m \text{ odd}. \tag{A.14}$$

(iv) $\sigma \in \widetilde{H}^{-1/2}(\mathbb{D}_1)$ *can be expanded on the basis* $\{y_l^m \omega^{-1} \,:\, l+m \,\mathbf{even}\}$ *of* L^2_{ω}*:*

$$\sigma(\mathbf{x}) = \sum_{l=0}^{\infty} \sum_{m=-l}^{l} \sigma_l^m \frac{y_l^m(\mathbf{x})}{\omega(\mathbf{x})}, \quad \sigma_l^m = (\sigma, \omega^{-1} y_l^m)_{\omega}, \quad l+m \text{ even}. \tag{A.15}$$

Proof. Since the bilinear form associated to W is symmetric, elliptic and continuous, it induces an energy inner product on $\widetilde{H}^{1/2}(\mathbb{D}_1)$. Then, the proof of (i) boils down to showing that for $u \in \widetilde{H}^{1/2}(\,\mathbb{D}_1)$

$$\langle W u \,,\, y_l^m \rangle_{\mathbb{D}_1} = 0, \; \forall l+m \text{ odd} \quad \Leftrightarrow \quad u \equiv 0$$

Use symmetry of the bilinear form and (A.4) to get

$$\langle W u\,,\, y_l^m\rangle_{\mathbb{D}_1} = \frac{1}{\lambda_l^m}\left\langle u\,,\, \frac{y_l^m}{\omega}\right\rangle_{\mathbb{D}_1} = \frac{1}{\lambda_l^m}(u, y_l^m)_{1/\omega},$$

which is zero $\Leftrightarrow u \equiv 0$ because $\{y_l^m\,:\, l+m$ **odd**$\}$ is an orthogonal basis for $L^2_{1/\omega}$.

The remaining 3 cases follow by analogy. □

REMARK 9. *One can prove that* **odd** *PSH can be factored as*

$$y_l^m(\mathbf{x}) = e^{im\theta_x}\omega(\mathbf{x})\Psi(\mathbf{x}), \quad l+m \text{ odd},$$

where Ψ is a polynomial function (Combine [5, Eq 14.3.21], [1, 3.2(7)], and [1, 10.9(22)]).

However, this is not true when $l+m$ is **even**. *In that case, the radial part of y_l^m is already a polynomial (since [1, 10.9(21)] holds instead of [1, 10.9(22)]).*

This property confirms that the basis functions of our four fractional Sobolev spaces have the correct behaviour. Namely, when $l+m$ is odd, $y_l^m \sim \omega$ near the boundary ($\in \widetilde{H}^{1/2}(\mathbb{D}_1)$); when $l+m$ is even, $y_l^m\omega^{-1} \sim \omega^{-1}$ near $\partial\mathbb{D}_1$ ($\in \widetilde{H}^{1/2}(\mathbb{D}_1)$); while the basis functions of $H^{1/2}(\mathbb{D}_1)$ and $H^{-1/2}(\mathbb{D}_1)$ have no singular behaviour.

DEFINITION A.3 (**Kinetic moments over** $\mathbb{D}_1$[23, eq.(51)]). *Define the operators $\mathcal{L}_+$ and $\mathcal{L}_-$ of derivation over $\mathbb{D}_1$ as*

$$\mathcal{L}_\pm\, u = e^{\pm i\theta}\left(\pm\frac{\partial u}{\partial r} + i\frac{1}{r}\frac{\partial u}{\partial \theta}\right). \tag{A.16}$$

PROPOSITION A.6 (**Properties of the kinetic moments over** $\mathbb{D}_1$[23, sl. 21, eq. (80)][26, Prop. 2.7.7, Cor. 2.7.2, Lemma 2.7.3]). *Let $u, v \in C^\infty(\mathbb{D}_1)$, and $\mathbf{x}, \mathbf{y} \in \mathbb{D}_1$. The kinetic moments satisfy over $\mathbb{D}_1$*

$$\underline{\mathrm{curl}}_{\mathbb{D}_1,\mathbf{x}}\, u(\mathbf{x}) \cdot \underline{\mathrm{curl}}_{\mathbb{D}_1,\mathbf{y}}\, v(\mathbf{y}) = -\frac{1}{2}\left(\mathcal{L}_{+,\mathbf{x}}\, u(\mathbf{x})\, \mathcal{L}_{-,\mathbf{y}}\, \overline{v(\mathbf{y})} + \mathcal{L}_{-,\mathbf{x}}\, u(\mathbf{x})\, \mathcal{L}_{+,\mathbf{y}}\, \overline{v(\mathbf{y})}\right), \tag{A.17}$$

together with $\mathcal{L}_+^* = \mathcal{L}_-$, and $\mathcal{L}_-^* = \mathcal{L}_+$. Moreover, when applied to PSH, we get

$$\mathcal{L}_+\, y_l^m(\mathbf{x}) = \sqrt{(l-m)(l+m+1)}\frac{y_l^{m+1}(\mathbf{x})}{\omega(\mathbf{x})}, \tag{A.18}$$

$$\mathcal{L}_-\, y_l^m(\mathbf{x}) = \sqrt{(l+m)(l-m+1)}\frac{y_l^{m-1}(\mathbf{x})}{\omega(\mathbf{x})}. \tag{A.19}$$

REMARK 10. *Due to Proposition A.5,* (A.18) *and* (A.19) *can also be interpreted as: $\mathcal{L}_\pm$ maps $H^{1/2}(\mathbb{D}_1)$ to $H^{-1/2}(\mathbb{D}_1)$, and $\widetilde{H}^{1/2}(\mathbb{D}_1)$ to $\widetilde{H}^{-1/2}(\mathbb{D}_1)$.*

Proof of Proposition 2.7 We begin our proof by introducing the following recursion formula

$$\frac{4}{\lambda_l^m} = \frac{1}{2}\left[(l+m)(l-m+1)\lambda_l^{m-1} + (l-m)(l+m+1)\lambda_l^{m+1}\right], \tag{A.20}$$

which can be verified by direct computations using the multiplicative property of the Gamma function,i.e., $\Gamma(z+1) = z\Gamma(z)$.

Plugging this recursion formula into (A.9) gives

$$(\overline{\mathsf{W}} y_l^m)(\mathbf{x}) = \frac{4}{\lambda_l^m} \frac{y_l^m(\mathbf{x})}{\omega(\mathbf{x})}$$
$$= \frac{1}{2}\left[(l+m)(l-m+1)\lambda_l^{m-1} + (l-m)(l+m+1)\lambda_l^{m+1}\right] \frac{y_l^m(\mathbf{x})}{\omega(\mathbf{x})}. \quad \text{(A.21)}$$

From (A.18) and (A.19), it is clear that

$$\mathcal{L}_+ \, y_l^{m-1}(\mathbf{x}) = \sqrt{(l-m+1)(l+m)} \frac{y_l^m(\mathbf{x})}{\omega(\mathbf{x})}, \quad \text{(A.22)}$$

$$\mathcal{L}_- \, y_l^{m+1}(\mathbf{x}) = \sqrt{(l+m+1)(l-m)} \frac{y_l^m(\mathbf{x})}{\omega(\mathbf{x})}. \quad \text{(A.23)}$$

Moreover, by unicity of $\mathsf{W}^{-1} = \overline{\mathsf{V}}$ [14, Prop. 2.2], it must hold that

$$(\overline{\mathsf{V}} \frac{y_l^{m\pm1}}{\omega})(\mathbf{x}) = \lambda_l^{m\pm1} y_l^{m\pm1}(\mathbf{x}), \quad l+m\pm1 \text{ odd}. \quad \text{(A.24)}$$

Then, combining all these ingredients, it is clear that for $(l,m) \neq (0,0)$, $l+m$ even[3], our expression is equivalent to

$$(\overline{\mathsf{W}} y_l^m)(\mathbf{x}) = \frac{1}{2}\left(\mathcal{L}_+ \, \overline{\mathsf{V}} \, \mathcal{L}_- \, y_l^m(\mathbf{x}) + \mathcal{L}_- \, \overline{\mathsf{V}} \, \mathcal{L}_+ \, y_l^m(\mathbf{x})\right).$$

It follows that the associated bilinear form is

$$\left\langle \overline{\mathsf{W}} y_{l_1}^{m_1} \, , \, y_{l_2}^{m_2} \right\rangle_{\mathbb{D}_1} = \frac{1}{2}\left(\left\langle \mathcal{L}_+ \, \overline{\mathsf{V}} \, \mathcal{L}_- \, y_{l_1}^{m_1} \, , \, y_{l_2}^{m_2} \right\rangle_{\mathbb{D}_1} + \left\langle \mathcal{L}_- \, \overline{\mathsf{V}} \, \mathcal{L}_+ \, y_{l_1}^{m_1} \, , \, y_{l_2}^{m_2} \right\rangle_{\mathbb{D}_1}\right)$$
$$= \frac{1}{2}\left(\left\langle \overline{\mathsf{V}} \, \mathcal{L}_- \, y_{l_1}^{m_1} \, , \, \mathcal{L}_- \, y_{l_2}^{m_2} \right\rangle_{\mathbb{D}_1} + \left\langle \overline{\mathsf{V}} \, \mathcal{L}_+ \, y_{l_1}^{m_1} \, , \, \mathcal{L}_+ \, y_{l_2}^{m_2} \right\rangle_{\mathbb{D}_1}\right), \quad \text{(A.25)}$$

for $(l_1, m_1) \neq (0,0)$ and $(l_2, m_2) \neq (0,0)$.

Finally, (A.17) and

$$\overline{\mathcal{L}}_\pm = -\,\mathcal{L}_\mp, \quad \text{(A.26)}$$

imply that (A.25) can be rewritten as the desired formula. □

It is worth noticing that the condition $(l,m) \neq (0,0)$ only excludes the constants, characterized by y_0^0. Due to the orthogonality (A.2), this space is defined by

$$H_*^{1/2}(\mathbb{D}_1) = \{v \in H^{1/2}(\mathbb{D}_1) \, : \, \left\langle v \, , \, \omega^{-1} \right\rangle_{\mathbb{D}_1} = 0\}.$$

Appendix B. Proof of Proposition 2.8.

Recall we want to prove

$$(\overline{\mathsf{W}} 1)(\mathbf{y}) = \frac{4}{\pi} \omega(\mathbf{y})^{-1}, \quad \mathbf{y} \in \mathbb{D}_1.$$

[3] $\frac{4}{\lambda_0^0} = \frac{1}{2}\left((0)(1)\lambda_0^{-1} + (0)(1)\lambda_0^1\right) = \frac{4}{\pi}\Gamma(0)0$ where it is crucial that $\lim_{s\to 0} \Gamma(s)s = 1$. In order to go from (A.20) to (A.21) one actually "splits this limit" and breaks the identity.

Proof. Let us rewrite the modified hypersingular operator acting on the constant function 1 as

$$\begin{aligned}(\overline{\mathsf{W}}1)(\mathbf{y}) &= \frac{2}{\pi^2}\int_{\mathbb{D}_1} k_{\overline{\mathsf{W}}}(\mathbf{x},\mathbf{y})d\mathbb{D}_1(\mathbf{x}) \\ &= \frac{4}{\pi}\int_{r_y}^1 \frac{s^2}{(s^2-r_y^2)^{3/2}}\int_0^s \frac{r_x}{(s^2-r_x^2)^{3/2}}dr_x ds, \end{aligned} \tag{B.1}$$

where in the second line [19, eq. (39)] was applied, with an appropriate scaling for (2.2). Based on Hadamard's finite part, we can derive the following two formulas:

$$\frac{d}{ds}\int_0^s \frac{r_x}{\sqrt{s^2-r_x^2}}dr_x = -s\int_0^s \frac{r_x}{(s^2-r_x^2)^{3/2}}dr_x, \tag{B.2}$$

and

$$\begin{aligned}\frac{d}{dr_y}\int_{r_y}^1 \frac{sf(s)}{\sqrt{s-r_y^2}}ds &= r_y\int_{r_y}^1 \frac{sf(s)}{(s^2-r_y^2)^{3/2}}ds \\ &= -\frac{r_y f(1)}{\sqrt{1-r_y^2}} + r_y\int_{r_y}^1 \frac{1}{\sqrt{s-r_y^2}}\frac{d}{ds}f(s)ds. \end{aligned} \tag{B.3}$$

Using these in our expression (B.1), we obtain

$$(\overline{\mathsf{W}}1)(\mathbf{y}) = -\frac{4}{\pi}\frac{1}{r_y}\frac{d}{dr_y}\int_{r_y}^1 \frac{s}{\sqrt{s-r_y^2}}\frac{d}{ds}\int_0^s \frac{r_x}{\sqrt{s^2-r_x^2}}dr_x ds.$$

We integrate the inner integral and get

$$\int_0^s \frac{r_x}{\sqrt{s^2-r_x^2}}dr_x = (-\sqrt{s^2-r_x^2})|_{r_x=0}^1 = s.$$

So our expression becomes

$$(\overline{\mathsf{W}}1)(\mathbf{y}) = -\frac{4}{\pi}\frac{1}{r_y}\frac{d}{dr_y}\int_{r_y}^1 \frac{s}{\sqrt{s-r_y^2}}ds,$$

where

$$\int_{r_y}^1 \frac{s}{\sqrt{s-r_y^2}}ds = \sqrt{1-r_y^2}.$$

Consequently

$$(\overline{\mathsf{W}}1)(\mathbf{y}) = \frac{4}{\pi}\frac{1}{\sqrt{1-r_y^2}},$$

as desired. □